Redox Biology 74 (2024) 103229

Contents lists available at ScienceDirect

Redox Biology

journal homepage: www.elsevier.com/locate/redox

Activation of Nrf2 inhibits atherosclerosis in *ApoE*$^{-/-}$ mice through suppressing endothelial cell inflammation and lipid peroxidation

Lei He [a,b], Qinghua Chen [a], Li Wang [a], Yujie Pu [a], Juan Huang [b,c], Chak Kwong Cheng [a], Jiang-Yun Luo [b], Lijing Kang [a], Xiao Lin [d], Li Xiang [e], Liang Fang [f], Ben He [f], Yin Xia [b], Kathy O. Lui [g], Yong Pan [h], Jie Liu [h], Cheng-Lin Zhang [h,**], Yu Huang [a,b,*]

[a] Department of Biomedical Sciences, City University of Hong Kong, Hong Kong, PR China
[b] School of Biomedical Sciences, Chinese University of Hong Kong, Hong Kong, PR China
[c] Shenzhen Key Laboratory of Cardiovascular Disease, Fuwai Hospital Chinese Academy of Medical Sciences, Shenzhen, PR China
[d] Department of Psychiatry, Icahn School of Medicine at Mount Sinai, New York, USA
[e] State Key Laboratory of Environmental and Biological Analysis, Department of Chemistry, Hong Kong Baptist University, Hong Kong, PR China
[f] Department of Cardiology, Shanghai Chest Hospital, Shanghai Jiao Tong University School of Medicine, Shanghai, PR China
[g] Department of Chemical Pathology, and Li Ka Shing Institute of Health Science, The Chinese University of Hong Kong, Hong Kong, PR China
[h] Department of Pathophysiology, School of Basic Medical Sciences, Shenzhen University Medical School, Shenzhen, PR China

ARTICLE INFO

Keywords:
Nuclear erythroid 2-related factor 2
Inflammation
Lipid peroxidation
Endothelial cells
Atherosclerosis

ABSTRACT

Background: Nuclear erythroid 2-related factor 2 (Nrf2), a transcription factor, is critically involved in the regulation of oxidative stress and inflammation. However, the role of endothelial Nrf2 in atherogenesis has yet to be defined. In addition, how endothelial Nrf2 is activated and whether Nrf2 can be targeted for the prevention and treatment of atherosclerosis is not explored.

Methods: RNA-sequencing and single-cell RNA sequencing analysis of mouse atherosclerotic aortas were used to identify the differentially expressed genes. *In vivo* endothelial cell (EC)-specific activation of Nrf2 was achieved by injecting adeno-associated viruses into *ApoE*$^{-/-}$ mice, while EC-specific knockdown of Nrf2 was generated in *Cdh5*^{Cre}*Cas9*$^{floxed\text{-}stop}$*ApoE*$^{-/-}$ mice.

Results: Endothelial inflammation appeared as early as on day 3 after feeding of a high cholesterol diet (HCD) in *ApoE*$^{-/-}$ mice, as reflected by mRNA levels, immunostaining and global mRNA profiling, while the immunosignal of the end-product of lipid peroxidation (LPO), 4-hydroxynonenal (4-HNE), started to increase on day 10. TNF-α, 4-HNE, and erastin (LPO inducer), activated Nrf2 signaling in human ECs by increasing the mRNA and protein expression of Nrf2 target genes. Knockdown of endothelial Nrf2 resulted in augmented endothelial inflammation and LPO, and accelerated atherosclerosis in *Cdh5*^{Cre}*Cas9*$^{floxed\text{-}stop}$*ApoE*$^{-/-}$ mice. By contrast, both EC-specific and pharmacological activation of Nrf2 inhibited endothelial inflammation, LPO, and atherogenesis.

Conclusions: Upon HCD feeding in *ApoE*$^{-/-}$ mice, endothelial inflammation is an earliest event, followed by the appearance of LPO. EC-specific activation of Nrf2 inhibits atherosclerosis while EC-specific knockdown of Nrf2 results in the opposite effect. Pharmacological activators of endothelial Nrf2 may represent a novel therapeutic strategy for the treatment of atherosclerosis.

1. Introduction

Atherosclerosis, a chronic inflammatory disorder is the leading cause of myocardial infarction, ischemic stroke, and peripheral vascular disease [1]. Endothelial inflammation induced by cytokines, oscillatory shear stress, oxidized low-density lipoprotein (ox-LDL), and free radicals, leads to the adhesion of monocytes to the activated endothelial cells (ECs), which facilitates the transformation of monocytes into foam cells [1,2]. In addition, a hyperinflammatory state can cause cell death, which compromises endothelial integrity and thus promotes the penetration of lipids into the subendothelial layer of the vasculature. Both animal studies and clinical trials have shown that neutralizing tumor

* Corresponding author. Department of Biomedical Sciences, City University of Hong Kong, Hong Kong, PR China.
** Corresponding author. Department of Pathophysiology, School of Basic Medical Sciences, Shenzhen University Medical School, Shenzhen, PR China.
E-mail addresses: zhangchenglin07@szu.edu.cn (C.-L. Zhang), yu.huang@cityu.edu.hk (Y. Huang).

https://doi.org/10.1016/j.redox.2024.103229
Received 4 April 2024; Received in revised form 22 May 2024; Accepted 5 June 2024
Available online 6 June 2024

necrosis factor α (TNF-α), interleukin-1β (IL-1β), and IL-6 were found to suppress inflammatory responses, which contributes to reduced plaque formation in athero-prone mice and to improved cardiovascular outcomes in patients with atherosclerosis [3–5].

Lipid peroxidation (LPO) closely related to oxidative stress can result in EC inflammation, apoptosis, and vascular dysfunction [6]. LPO is triggered by excessive accumulation of reactive oxygen species (ROS) and depletion of glutathione (GSH) in the phospholipids of cell membranes. These membranes are rich in polyunsaturated fatty acids and are therefore rapidly oxidized, leading to the formation of harmful by-products particularly 4-hydroxynonenal (4-HNE) [7]. Elevation of LPO end-products has been reported in Alzheimer's disease, cancer, diabetes, and atherosclerosis [8–11]. Previous studies showed that LPO inhibitors such as ferrostatin-1 or an iron chelator can effectively inhibit atherosclerosis through reducing LPO and improving endothelial function in the *ApoE*$^{-/-}$ mouse aortas [11,12].

The transcription factor nuclear factor (erythroid-derived 2)-like 2 (Nrf2) is a critical regulator of redox balance, pentose metabolism, and inflammatory responses [13]. Under physiological conditions, Nrf2 bound by Keap1 (Kelch-like ECH-associated protein 1) in the cytoplasm undergoes constant ubiquitination and proteasomal degradation [13]. When cells are under stress or exposed to oxidants and electrophile agents, such as 4-HNE, the cysteine thiol residues of Keap1 can be modified to relieve its inhibitory effect on Nrf2 [14], while the newly synthesized Nrf2 is no longer degraded by Keap1 and it is then translocated into the nucleus to initiate transcription of antioxidant response element (ARE)-containing genes [15]. Nrf2 target genes include glutamate-cysteine ligases (GCLs), solute carrier family 7 member 11 (SLC7A11), SLC3A2, and glutathione peroxidase 4 (GPX4) involved in GSH metabolism. Furthermore, Nrf2 regulates iron/heme metabolism by increasing the expression of heme oxygenase-1 (HMOX1) and ferritin light/heavy chain 1 (FTL/FTH1). Moreover, Nrf2 enhances the gene expression of NAD(P)H quinone dehydrogenase 1 (NQO1) and thioredoxin reductase 1 (TXNRD1), which are essential for reducing oxidized protein thiols and mediating xenobiotic detoxification.

Due to its multifaceted roles, Nrf2 has been implicated in maintaining redox homeostasis, regulating inflammatory responses, controlling lipid metabolism, influencing macrophage polarization and foam cell formation during atherosclerosis [16]. Nrf2 is reported to inhibit inflammation through multiple mechanisms. For example, Nrf2 binds to the ARE sequence on the promoter region of IL-1β and IL-6 and thus suppresses their transcription in macrophages [17,18]. Nrf2 activation is found to reduce the expression of VCAM-1 and MCP-1 through inhibiting the MKK6-p38 MAPK signaling in endothelial cells [19,20]. The ectopic expression of Nrf2 inhibits the proliferation of vascular smooth muscle cells [21]. However, Nrf2 expression in macrophages may paradoxically expedite the progression of atherosclerosis by upregulating CD36 expression, thus facilitating lipid uptake and foam cell formation. The Nrf2 global knockout mice on an *ApoE*$^{-/-}$ background developed fewer atherosclerotic plaques [22]. On the other hand, transplantation of bone borrow cells derived from *Nrf2*$^{+/+}$/*ApoE*$^{-/-}$ mice into *Nrf2*$^{-/-}$/*ApoE*$^{-/-}$ mice was found to be pro-atherogenic [23], indicating a role of Nrf2 in bone marrow cells during the progression of atherosclerosis in *ApoE*$^{-/-}$ mice. By contrast, transplantation of bone marrow cells from Nrf2$^{-/-}$ mice into *LDLR*$^{-/-}$ mice resulted in larger atherosclerotic lesions probably due to the increased foam cell formation and pro-inflammatory macrophages at both early and late stages of atherosclerosis [24]. These contradictory results suggest that the impact of Nrf2 in atherogenesis is likely dependent on cell type and genetic background. However, there is currently no direct evidence for a role of endothelial Nrf2 in the pathogenesis of atherosclerosis.

The present study aimed to investigate the involvement of endothelial Nrf2 in atherogenesis in *ApoE*$^{-/-}$ mice and to determine the timing and mechanism of endothelial Nrf2 activation during the initial phase of atherosclerosis in relation to inflammation and LPO. Furthermore, we evaluated the potential of dimethyl itaconate (DMI), an Nrf2 activator, as a therapeutic agent for the prevention and treatment of atherosclerosis.

2. Methods

2.1. Animals

Apolipoprotein E deficient (*ApoE*$^{-/-}$) mice, *Cdh5*^{Cre}*Cas9* $^{floxed\text{-}stop}$*ApoE*$^{-/-}$ mice, and *Cas9* $^{floxed\text{-}stop}$*ApoE*$^{-/-}$ mice were provided by the Laboratory Animal Services Centre at Chinese University of Hong Kong, and their usage was approved by the Animal Research Ethical Committee (Ref No. 20-055-GRF). The mice were housed in temperature-controlled cages with a 12/12-hr light/dark cycle and had free access to water and a standard chow diet unless otherwise stated. The endothelial cell-specific Cas9 overexpression mice (*EC-Cas9*) were generated by breeding male *Cdh5*^{Cre} mice (Jackson Laboratories, B6; 129-Tg (Cdh5-Cre)1Spe/J) with female Rosa26-LSL-Cas9 (Cas9$^{floxed\text{-}stop}$) mice (Jackson Laboratories, Gt (ROSA)26Sor$^{tm1.1(CAG\text{-}cas9_{*},\text{-}EGFP)Fezh}$/J, #024857). The 8-week-old mice were then mated with *ApoE*$^{-/-}$ mice to generate ECs-specific expressing Cas9 simultaneously (*Cdh5*^{Cre} *Cas9* $^{floxed\text{-}stop}$*ApoE*$^{-/-}$) mouse lines. Male *Cdh5*^{Cre}*Cas9* $^{floxed\text{-}stop}$*ApoE*$^{-/-}$ mice aged at 10–12 weeks were randomly assigned to two groups; they were injected with EC-enhanced AAV9-mNrf2-sgRNA (AAV-sgNrf2) or EC-enhanced AAV9-vector (AAV-Vector) (1×10^{12} gc/mice) via tail vein. The mice were then maintained for 3 weeks to generate EC-specific Nrf2 knockdown mice. The mice were then fed on an HCD for 8 weeks. To generate EC-specific Keap1 knockdown mice, AAV-*vector* or AAV-sg*Keap1* (1×10^{12} gc/mice) were administered to male and female *ApoE*$^{-/-}$ mice (10–12 weeks) via tail vein injection and maintained for 3 weeks. The mice were then fed with an HCD for 8 weeks. *ApoE*$^{-/-}$ mice aged 10–12 weeks were intragastrically administered with 100 mg/kg/day of dimethyl itaconate (DMI, Sigma-Aldrich, 617-52-7) or H_2O for 2 or 4 weeks. Atherosclerotic mice were induced by feeding them an HCD containing 60 kcal % fat (Research Diets, D12336, USA). Body weight was monitored weekly during the treatment. Drugs and chemicals used are listed in Supplemental T able 1.

2.2. Cell culture

Human umbilical vein endothelial cells (HUVECs) obtained from Lonza (C2591A) were cultured in EGM (DMEM/F12 supplemented with 20 % FBS, ECGS (10 μg/mL), and 100 U/mL penicillin plus 100 μg/mL streptomycin) at 37 °C. Human aortic endothelial cells (HAECs) were provided by Invitrogen (C-006-5C) and cultured in Medium 200 (Gibco, M200500) with low serum growth supplement kit (Thermo fisher scientific, S003K). HEK293T cells from ATCC (CRL-3216™) were cultured in a high glucose DMEM (Thermo Fisher Scientific, 12100046) supplemented with 10 % FBS. The THP-1 cells (ATCC® TIB-202™) were cultured in RPMI-1640 medium (Gibco, 31800105) supplemented with 2-mercaptoethanol (Gibco, 21985023) to a final concentration of 0.05 mM and 10 % FBS.

2.3. Construction of endothelial cell-specific AAV-mediated plasmid

To generate single guide RNAs (sgRNAs) for SpCas9 and SaCas9 targets, the CRISPR design tool (CRISPR/Cas9 target online predictor, CCTop (https://cctop.cos.uni-heidelberg.de:8043/index.html) [25]) was used to select the three 20-nt target sequences preceding a 5′-NGG of a protospacer-adjacent motif sequence of mouse Nrf2 CDS. The annealed oligos were then cloned into the pAAV-U6-sgRNA-CMV-GFP (Addgene, #85451) using *Sap*I. To generate Keap1 *in vivo* genome editing, the pX601-AAV-CMV: NLS-SaCas9-NLS-3xHA-bGHpA; U6*Bsa*I sgRNA (gifted from F. Zhang, Addgene plasmid, #61591) was utilized. The primers used for the preparation of sgNrf2 and sgKeap1 are listed in Supplemental Ta ble 2.

2.4. Endothelium-enhanced AAV packaging

The RGDLRVS-AAV9-cap plasmid (gifted from Dr. O.J. Müller, University Hospital Heidelberg, Heidelberg, Germany) was utilized to package recombinant endothelial enhanced AAV due to its high infection efficiency in endothelium [26]. A plasmid cocktail containing the resulting plasmid, AAV9 packaging plasmid, and p-Helper envelope plasmid was co-transfected into HEK293T cells using polyethyleneimine (PEI). The medium was changed 16 h after transfection. 3–5 days after transfection, the supernatant was removed and the cells pellet was suspended with Tris-NaCl Buffer. The cells were frozen (−80 °C, 30 min) and thawed (37 °C, 15 min) for 3 cycles to release the virus. The resulting samples were spun and the supernatant was transferred into fresh tubes, followed by precipitation with polyethylene glycol 6000, purified by chloroform, and suspended in PBS containing 4 % sucrose. Finally, the virus was aliquoted and stored at −80 °C. The AAV titer was determined using qPCR, following the titration protocol provided by Addgene.

2.5. Lentivirus production

The human *Nrf2* shRNA sequence was cloned into the pLKO.1 plasmid backbone. The primers used for shNrf2 preparation are listed in Supplemental Ta ble 2. The human *Keap1* shRNA was purchased from Genechem Station (Shanghai, China). Lentivirus encoding Nrf2 shRNA (LV-shNrf2) and Keap1 shRNA (LV-shKeap1) was generated by transfecting a plasmid cocktail containing the shuttle plasmid pLKO.1 (Addgene, #10878), the packaging plasmid psPAX2 (Addgene, #12260), and the envelope plasmid pMD2.G (Addgene, #12259) into HEK293T cells. The medium was changed 15 h after transfection. The medium containing LV-SCR or LV-shNrf2 or LV-shKeap1 was harvested 48 h and 72 h after transfection. The cell debris was removed by passing the medium through 0.45 μm filters. The virus was then precipitated with polyethylene glycol 6000, purified by chloroform and suspended in PBS containing 4 % sucrose. The virus was aliquoted and stored at −80 °C.

2.6. Isolation of mouse aortic endothelial cells

After sacrifice by CO_2 euthanasia, the mouse aortas were dissected out and put in cold PBS. A 23-gauge needle was inserted into the aorta and clamped tightly with forceps. The vessel lumen was perfused with 1 mL of QIAzol Lysis reagent (Qiagen,79,306) within 1 min via a plastic catheter. The cells that were washed away by the lysis reagent were mostly endothelial cells, while vascular smooth muscle cells comprised the majority of the remaining aortic tissue. The successful isolation of endothelial cells was confirmed using qPCR by the use of markers for both endothelial and smooth muscle cells.

2.7. Isolation of lung endothelial cells

The mice were sacrificed by CO_2 euthanasia. The left atrium was cut open before perfusing the right ventricle with sterile PBS to clear the blood in the lungs. The lung tissues were then cut into small pieces and processed with 10 mL of 450 U/mL of type I collagenase (Worthington, LS004194) and 60 U/mL of deoxyribonuclease I (Worthington, LS006333) in Hank's Balanced Salt Solution or serum-free medium (DMEM/F12). To stop the digestion, an equivalent volume of FACS buffer (sterile PBS with 2 mmol/L EDTA plus 2 % FBS plus 100 U/mL penicillin plus 100 g/mL streptomycin) was added. To remove undigested tissue, cells were filtered through a 70 μm strainer and centrifuged. The cell pellet was resuspended in 200 μL of FACS buffer, followed by addition of 1:20 CD31 microbeads (Miltenyi Biotec, 130-097-418). After incubation on ice, each sample was mixed with 2 mL of FACS buffer and centrifuged to remove the supernatant. The cell pellet was resuspended in FACS buffer for the second time and loaded onto an LS column (Miltenyi Biotec, 130-042-401) that had been pre-washed with FACS buffer. The column was washed twice with additional FACS buffer before being removed from the magnet and placed on the top of a tube. The beads on the column were washed with FACS buffer by pushing the syringe plug when there was approximately 1 mL remaining. The collected solution was centrifuged, and the resulting cell pellet was identified as $CD31^+$ lung microvascular ECs.

2.8. Dual luciferase activity assay

A pGL3-NF-κB reporter plasmid containing a firefly luciferase gene was used. HUVECs were plated overnight in a 24- well plate and then transiently transfected with a purified pGL3-NF-κB luciferase plasmid along with an internal control plasmid *Renilla* by using the Neon Transfection System (Thermo Fisher Scientific). After 6 h, the culture medium was replaced with fresh F12 supplemented with 20 % FBS. The cells were then pretreated with DMI (100 μM) for 3 h and incubated with TNF-α (10 ng/mL) for 24 h. The activities of firefly and *Renilla* luciferase were determined according to the manufacturer's instructions (Promega, #E1960). Briefly, the cells were washed twice in PBS and lysed in 1 × passive lysis buffer for 15 min at room temperature with gentle shaking. 10 μL of cell lysate was transferred to 1.5 mL EP tube and subsequently mixed with 50 μL of LAR II buffer. The activity of firefly luciferase was determined using a GloMaxR-20/20 single-tube Luminometer (Promega). The ratio of luciferase activity was calculated based on the activity of firefly luciferase and *Renilla* luciferase.

2.9. Hemodynamics study in vitro

The Ibidi flow system (Ibidi, Germany) was used in conjunction with self-made flow chambers to generate oscillatory shear stress (OSS) at 4 ± 0.5 dyne/cm^2 and 1 Hz. The flow system was assembled, and the computer control program was set up in accordance with the manufacturer's instructions. HUVECs were seeded onto a 75 mm × 38 mm glass slide (Corning) pre-coated with fibronectin (50 μg/mL). After a 12-h growth period on the glass in medium containing 10 % FBS, the slide was then mounted onto the custom-built flow chamber and connected to the Ibidi flow system with 2 % FBS-EGM. The cells were then exposed to OSS for varying durations, as indicated [27,28].

2.10. Oil red O staining for atherosclerotic plaques

Mice were euthanized using CO_2 and the entire aortas, including the aortic arch, thoracic, and abdominal segments, were dissected out and cut open longitudinally to expose the atherosclerotic plaques. The plaques were then fixed overnight in 4 % formaldehyde at 4 °C. The aortic tissue was washed three times in PBS with a 10-min interval between wash and then rinsed in 60 % isopropanol. The aortas were stained with Oil Red O (O0625, Sigma) for 15 min, rinsed with 60 % isopropanol until the background became transparent, and then mounted with gelatin on cover slides for long-term storage. Images were recorded for subsequent analysis. The percentage of plaque area was determined using National Institutes of Health ImageJ software and calculated by expressing the plaque area relative to the total vascular area.

2.11. Immunohistochemical staining

HUVECs were seeded onto glass and fixed in 4 % paraformaldehyde for 10 min. Subsequently, they were permeabilized with 0.01 % Triton X-100 for an additional 10 min. The cells were then blocked with 5 % bovine serum albumin (BSA) in PBS at room temperature for 1 h. Afterward, the indicated primary antibody was added and incubated overnight at 4 °C, followed by the corresponding Alexa Fluor® secondary antibodies (1:500) for 2 h at room temperature in the dark. Finally, nuclei were stained with 10 μg/mL 4′,6-diamidino-2-phenylindole (DAPI, Invitrogen) in PBS for 10 min. For mouse aortas, the

cryosections of tissue slices were rinsed in PBS and the specimens were fixed with pre-cooled acetone for 15 min on ice. The slides were then rinsed three times in PBS with an interval of 5 min, blocked with 5 % BSA in PBS at room temperature for 60 min, and then incubated with diluted primary antibodies (antibody information is summarized in Supplemental Ta ble 3) overnight at 4 °C. The slides were left at room temperature for 20 min, rinsed three times in PBS, and incubated with the corresponding AlexaFluor secondary antibodies (1: 500) in room temperature for 2 h in the dark. After rinsing the slides three times in PBS at 5-min intervals, they were mounted with a coverslip using anti-fade mounting medium with DAPI (Beyotime, P0131). The coverslips were then sealed with nail polish to prevent drying. The slides were stored in the dark at −20 °C for one week or at 4 °C for 2 days. The Fluoview FV1200 laser scanning confocal system (Olympus, Tokyo, Japan) was used to capture fluorescent images.

2.12. Human artery samples and immunofluorescence staining of 4-HNE, TFRC and Nrf2

Carotid arteries were dissected from patients who underwent carotid endarterectomy while aortas were dissected from patients with abdominal or thoracic aortic aneurysms. The samples were obtained from Shanghai Chest Hospital, Shanghai Jiao Tong University School of Medicine. The specimens were fixed in a 4 % paraformaldehyde solution in PBS and then embedded in paraffin. For immunofluorescence staining, the paraffin-embedded samples were sliced into cross sections of 5 μm. The study was approved by the ethics committee of clinical research at Shanghai Jiao Tong University School of Medicine (Ref. NO.: IS21014). Before enrolling in the study, all participants signed an informed consent form.

Immunofluorescence staining for 4-HNE and TFRC was performed on paraffin sections of human carotid arteries, while aortas were stained for Nrf2. The tissue slices were dewaxed in xylene and gradient ethanol (100 %, 95 %, 80 %, and 70 %) before being subjected to 10 mM citrate buffer (pH 7.4) for antigen retrieval. Following blocking with 5 % BSA at room temperature for 1 h, the remaining steps were carried out as described above.

2.13. Measurement of ROS

The intracellular ROS level was measured using the dihydroethidium (DHE, Invitrogen, D11347) assay kit following the manufacturer's instructions. SCR or shNrf2-HUVECs were seeded on glass and incubated in the dark with 5 μM DHE in Krebs buffer at 37 °C for 30 min. Excess probe was removed with fresh F12 medium. Fluorescent images were captured using the Fluoview FV1200 laser scanning confocal system (Olympus, Tokyo, Japan).

The intracellular ROS level was also quantified by using the indicator CM-H2DCFDA (Invitrogen, C6827) according to the manufacturer's instructions. HUVECs were plated overnight in a 6-well plate and incubated with DMI (100 μM) for the indicated time points. CM-H2DCFDA was reconstituted to make a concentrated stock solution and kept tightly sealed until use. HUVECs were incubated in the dark for 30 min at 37 °C with 1 mM CM-H2DCFDA in prewarmed HEPES buffer. The excess probe was washed away with HEPES. Digested cells were resuspended in 200 μL of prewarmed HEPES and the resulting samples were placed in a 5 mL polystyrene round-bottom tube and analyzed using a cell analyzer (BD LSRFortessa, USA).

2.14. Cytoplasmic and nuclear protein extraction

The NE-PER Nuclear and Cytoplasmic Extraction Kit (Thermo, 78,833) was used. Briefly, the cells were collected and washed twice in sterile ice-cold PBS, followed by centrifugation at 3000 rpm for 5 min at 4 °C to collect the cell pellet. To resuspend cells in a tube, 100 μL of cytoplasmic extraction reagent I was added. The tube was then vortexed vigorously on the highest setting for 15 s to fully suspend the cell pellet. After incubating on ice for 10 min, 5.5 μL of cytoplasmic extraction reagent II was added. The tube was vortexed for 5 s at the highest setting. The samples were then centrifuged for 10 min at 12,000 rpm at 4 °C after being incubated on ice for 1 min and vortex for an additional 5 s. The supernatant cytoplasmic fraction was immediately transferred to a fresh pre-cooled 1.5 mL tube, while the nuclear fraction was washed once in pre-cooled PBS and the nuclear pellet was resuspended in 50 μL RIPA buffer for 30 min on ice with vertexing every 10 min. The pellet was ultrasonicated three times, each for 3 s, and centrifuged for 20 min at 12,000 rpm at 4 °C. The resulting supernatant (nuclear fraction) was collected and placed in a fresh pre-chilled tube.

2.15. Western blotting

The cells were homogenized in RIPA lysis buffer consisting of RIPA solution, protease inhibitors and phosSTOP phosphatase inhibitors (Roche, USA, 04,906,845,001). The amount of protein in the protein supernatant was determined using a BCA protein assay kit (Thermo Scientific, 23,225). An equal amount of protein was loaded onto SDS-PAGE along with the pre-stained protein marker (Thermo, #26616). The separated proteins were transferred to PVDF (Millipore, USA) using a Bio-Rad *Trans*-Blot® cell with wire electrodes, following the manufacturer's guidelines. The membranes were then blocked with 3 % bovine serum albumin dissolved in 1 × TBST buffer for 1 h at room temperature before being incubated with primary antibodies overnight at 4 °C. After being rinsed three times in TBST, the membranes were incubated with the corresponding secondary antibodies conjugated with horseradish peroxidase at room temperature for 2 h. They were then washed three times in 1 × TBST with 10-min intervals before being visualized using chemiluminescent HRP substrate (Millipore, USA). The protein bands observed by the Bio-rad chemiDoc imager were analyzed using Quantity One software.

2.16. Quantitative PCR analysis

RNA was extracted from tissue or cellular samples using RNAiso plus (Takara, #9109). 1000 ng of RNA was reverse transcribed into cDNA using PrimeScript RT Master Mix (Takara, RR036A). The targeted genes were detected using primers and cDNA with TB Green Premix Ex Taq (Takara, # RR420A) and analyzed through qPCR analysis on the ViiATM7 real-time PCR system (Applied Biosystems) following the manufacturer's protocol. The gene expression in cells was analyzed using the comparative C_T method with GAPDH or HSP90ab1 serving as the internal control.

2.17. RNA-sequencing

SCR- and shNrf2-HUVECs as well as HUVECs, were pretreated with DMI (100 μM) for 3 h and were then treated with TNF-α (10 ng/mL) for 12 h before cell harvesting for RNA extraction using the RNeasy Mini Kit (Qiagen, Germany). For mouse aortic endothelial cells, RNA extraction was performed after cell isolation. The extracted RNA samples were sent to the Novogene (Novogene Co., Ltd, Beijing, China) for RNA-sequencing analysis. The annotation file and reference genomes were referred to the ENSEMBL database. By utilizing Bowtie2 v2.2.3, the genome index was constructed. Using HISAT2v2.1.0, the genome index and the clean data were subsequently aligned to the reference genome. All samples have a fold coverage ranging from 24 to 40 (median: 33). The expression level of genes in each sample was estimated using FPKM (fragments per kilobase million mapped reads) after reads were enumerated with HTSeq v0.6.0. Genes were classified as differentially expressed if they met the criteria of $P < 0.05$ and a fold change higher than 1.5. GSEA tools were used for enrichment analysis and to identify key hub genes related to the phenotypic traits during the initiation of atherogenesis, a system biology approach called weighted gene co-

expression network analysis (WGCNA) was used to analyze gene clusters (modules). We used droplet-based scRNA-seq to analyze the entire mouse aorta as previously described [29]. Briefly, scRNA-seq data from the entire mouse aorta of our previous study, available at NCBI BioProject (accession number: PRJNA712944), was used. This scRNA-seq data was processed and re-analyzed for cell type clustering and differential gene expression analysis between normal chow diet (NCD) and high cholesterol diet (HCD) groups, with the following major settings: (1) cell filtering was conducted as previously reported in our previous study [29]; (2) the first 14 principal components were used for dimension reduction by uniform manifold approximation and projection (UMAP); (3) cell clustering was performed by using the first 14 principal components at a resolution of 0.1; (4) differential gene expression analysis was conducted between NCD and HCD groups for each cluster, using the "FindMarkers" function ("min.pct" set at 0.5); and (5) fold-changes of genes between NCD and HCD groups for each cluster were calculated, using the "FindMarkers" function ("min.pct" and "logfc.threshold" set at 0).

2.18. Monocyte attachment assay

HUVECs were pretreated with DMI (100 μM) for 3 h followed by TNF-α (10 ng/mL) for 12 h. For SCR-, shNrf2-or shKeap1-HUVECs, the cells were treated as indicated. THP-1 cells were cultured in RPMI 1640 medium. Thereafter, the cells were washed in PBS to remove cell debris and 2 mL of THP-1 monocyte suspension (10^5 cells/mL) was added to HUVECs. Non-adherent THP-1 cells were removed, followed by gentle wash of the cells in PBS and finally in fresh F12-EGM medium. The THP-1-bound HUVECs were visualized under a bright-field microscopy [28].

2.19. GSH/GSSG measurement

HUVECs were plated at a density of 1×10^6 cells per mL in a 10-cm dish. The cells were pre-treated with DMI (100 μM) for 1, 3 and 12 h and with hydrogen peroxide (100 μM) for 1 h. The cell medium was removed, and the levels of reduced glutathione (GSH) and oxidized glutathione (GSSG) were measured according to the manufacturer's instructions (Invitrogen, EIAGSHC). Briefly, the cell pellets were washed in ice-cold PBS and resuspended in 500 μL of ice-cold 5 % SSA (5-sulfosalicylic acid dihydrate, Sigma, S2130). The cells were lysed through vigorous vertexing followed by freeze-thaw cycling (−80 °C, 30 min →37 °C, 15 min) three times. Subsequently, they were incubated at 4 °C for 10 min. The samples were then centrifuged at 14,000 rpm for 10 min at 4 °C and the supernatant was collected for biochemical analysis. To measure total GSH, the standards and samples were diluted by adding four volumes of 1 × assay buffer. The reaction mixture was prepared by thoroughly mixing the glutathione reductase and NADPH. To measure GSSG, the standards and samples were diluted with sample dilution buffer containing 2VP (2-vinylpyridine, Sigma, 132,292). Next, 50 μL of diluted samples were added to wells, followed by addition of 25 μL of colorimetric detection reagent and 25 μL of reaction mixture. The plate was taped and mixed well and thereafter incubated at room temperature for 20 min. The absorbance at 450 nm was measured using a Microtiter plate reader (Bio-Rad, USA). The concentration of GSH and GSSG was calculated using the standard curve method and corrected by the protein concentration of each sample.

2.20. Liperfluo staining

Liperfluo (Dojindo.co., Japan) was used to detect lipid peroxide in living cells. Briefly, HUVECs were plated at a density of 1×10^5 cells in a 35 mm glass bottom dish (Thermo, 150,682) and cultured overnight. The medium was then replaced with fresh medium containing liperfluo (1 μM) and incubated at 37 °C for 30 min in 5 % CO_2 culture incubator. After incubation, the medium was discarded and replaced with pre-warmed fresh medium. The fluorescent images of the cells were captured using the filter channel of FITC (GFP, Alexa488) on the Fluoview FV1200 laser scanning confocal system.

2.21. Statistical analyses

The results represented the means and standard deviations (means ± SD) of n separate experiments. GraphPad Prism (Version 9.0, CA, USA) was used to analyze the data. Gene and protein expression were normalized to GAPDH or Hsp90ab1. Normality and equal variance tests were performed for all variables before further analysis. For data that passed equal variance test, an unpaired *t*-test was used to determine differences between two groups. For the analysis of differences in multiple groups, we used either one-way or two-way ANOVA followed by Tukey's multiple comparison test. If a normal distribution was not achieved, nonparametric tests were used. For comparing two independent groups, we applied the Mann-Whitney test and for comparing multiple groups, we used the Kruskal-Wallis's test followed by Dunn's multiple comparison test. $p < 0.05$ was considered as statistically significant.

3. Results

3.1. Endothelial Nrf2 signaling was activated at both the initial and advanced stages of atherosclerosis

In human aortas with intimal thickening, the expression of Nrf2 in the endothelium was higher compared to plaque-free aortas (Fig. 1A&1B). Similar results were observed in the advanced atherosclerotic aortas of *ApoE*$^{-/-}$ mice fed with HCD for 20 weeks. Single cell RNA sequencing showed that among the five Nrf2-regulated cytoprotective defensive systems, the genes related to GSH production and regeneration, TXN-based antioxidant system, NADPH regeneration, and heme and iron metabolism were upregulated in ECs (Fig. 1C). To determine the activation of Nrf2 signaling during the progression of atherosclerosis, *ApoE*$^{-/-}$ mice were fed with HCD for 3, 7, 10, 14, and 28 days (Fig. 1D). EC and non-EC components were then isolated from mouse aortas. The efficacy of EC purification was confirmed by the mRNA expression level of the endothelial marker *Cadherin 5* (*Cdh5*) (Supplemental F igure 1A) and the smooth muscle cells (SMCs) marker *Calponin* (*Cnn1*) (Supplemental Fi gure 1B). On day 3, the total plasma cholesterol level increased (Supplemental F ig. 1C&1D). Lipid deposits in the ascending aortas were not detected until day 7, as shown by Oil red O staining (Supplemental Fi gure 1E). In aortic ECs of HCD-fed *ApoE*$^{-/-}$ mice, the mRNA levels of Nrf2 target genes, *Hmox1*, *Slc7a11*, and *Gstm5* began to increase on day 14 (Fig. 1E). The GSEA analysis of the RNA sequencing data also revealed significant activation of Nrf2 pathway (Fig. 1F). Immunofluorescent staining showed that the protein level of Nrf2 was lower in ECs than that of SMCs in the aortas of NCD-fed *ApoE*$^{-/-}$ mice. However, it increased significantly on day 14 post HCD feeding (Fig. 1G & 1H). These findings suggest that endothelial Nrf2 was activated in both the initial and advanced stages of atherosclerosis.

3.2. Endothelial inflammation and LPO contributed to Nrf2 activation during atherogenesis

To investigate the molecular mechanism underlying the activation of endothelial Nrf2, we conducted RNA sequencing of the EC and non-EC components of the HCD-fed *ApoE*$^{-/-}$ mice aortas and performed the Weighted Correlation Network Analysis (WGCNA) analysis. We identified three clusters of genes (highlighted in red, black, and green) with the strongest correlation to the feeding duration of HCD, indicating that they may be the crucial hub genes associated with the severity of atherosclerosis (Supplemental F ig. 2A&2B). Further analysis of these genes in the three modules revealed enrichment in Th17 cell differentiation, TNF-α signaling pathway, JAK-STAT pathway, cytokine-cytokine receptor interaction, cholesterol metabolism, and chemokine

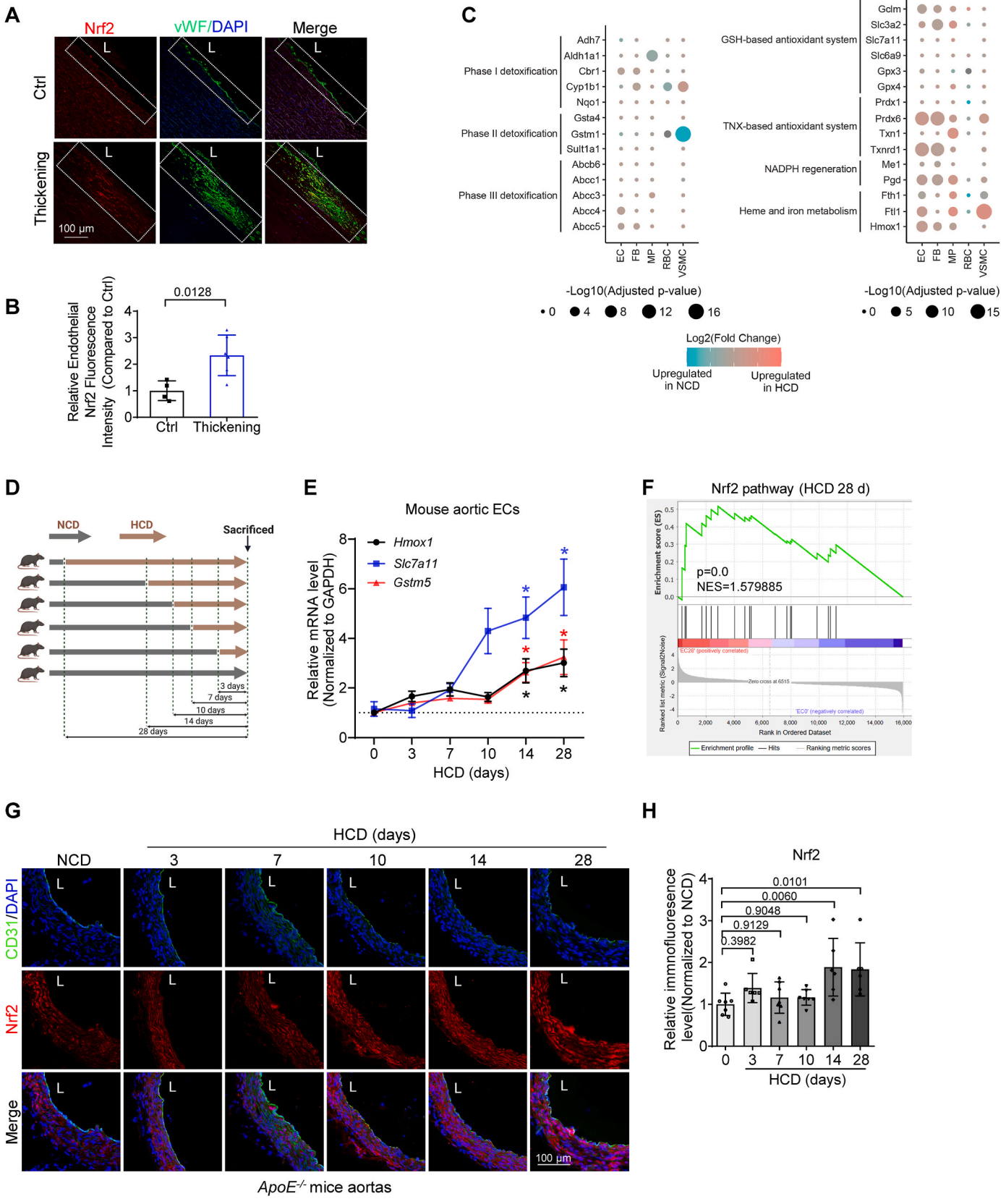

(caption on next page)

Fig. 1. Endothelial Nrf2 signaling was activated during atherogenesis.
(A & B) Representative immunofluorescence images and statistical analysis of Nrf2 (red) in human aortas with intimal thickening. The EC marker vWF (green) was used. n = 6. (C) Dot plots showed the signatures of Nrf2 target genes from scRNA sequencing data in aortas of *ApoE*$^{-/-}$ mice after 20-week high cholesterol diet (HCD) feeding. (D) A schematic diagram of the protocol for feeding mice with normal chow diet (NCD) or HCD for 3, 7, 10, 14 and 28 days was included. (E) ECs were isolated for qPCR to profile the expression of Nrf2 targeted genes (n = 6–8). (F) GESA analysis of the RNA sequencing results of EC components showed significant enrichment of Nrf2 signaling. (G) Representative immunofluorescence images of Nrf2 (in red) and CD31 (in green) in the ascending aorta of *ApoE*$^{-/-}$ mice were shown. (H) Statistical analysis of the results in (G), n = 6–7. Results are means ± SD. Statistical analysis was performed using an unpaired two-tailed Student's *t*-test for (B), and one-way ANOVA followed by Tukey's test for (E) and (H). L, lumen. (For interpretation of the references to color in this figure legend, the reader is referred to the Web version of this article.)

signaling pathway (Supplemental F igure 2C). This suggests that endothelial inflammation is critically associated with the development of atherosclerosis, which is consistent with the classic theory [30,31]. GSEA and KEGG analysis revealed that the inflammatory response was activated in the aortas in a time-dependent manner following HCD feeding (Fig. 2A, Supplemental Fi gure 2D). The expression of inflammatory genes (*Vcam1*, *Tnfa* and *Ccl2*) in ECs was confirmed by qPCR and immunofluorescence staining (Fig. 2B & 2C, Supplemental Fi gure 2E). These findings suggest that endothelial inflammation may occur before day 3 after HCD feeding, which is much earlier than previously thought [32].

LPO is a critical mediator of atherosclerosis. We stained the aortas of HCD-fed *ApoE*$^{-/-}$ mice with an antibody targeting 4-HNE-modified proteins. 4-HNE was nearly undetectable in both aortic ECs and SMCs of *ApoE*$^{-/-}$ mice on normal chow diet (NCD). However, its staining intensity gradually increased, reaching statistical significance on day 10, especially in the endothelial layer (Fig. 2B&2C). In carotid endarterectomy plaques from humans, higher levels of endothelial LPO were detected in the plaque lesions compared to plaque-free areas, as reflected by immunosignals of 4-HNE and transferrin receptor (TFRC), which is another marker of LPO [33,34] (Fig. 2D-2F).

To investigate whether inflammation and LPO have a causal link to Nrf2 activation, we treated HUVECs with TNF-α (10 ng/mL, 12 h), 4-HNE (100 μM), and erastin (20 μM, an LPO inducer) for indicated periods of time. TNF-α, 4-HNE, and the LPO inducer erastin alone were sufficient to significantly upregulate the expression of Nrf2 and its target genes, such as *HMOX1*, *TXNRD1*, *SLC3A2*, suggesting that EC inflammation and LPO are involved in the activation of Nrf2 (Fig. 2G-2J, Supplemental F ig. 3A&3G&3H). Exposure to 4-HNE at concentration over 50 μM resulted in significant death of HUVECs (Supplemental Fi gure 3B). By contrast, the LPO inhibitor ferrostatin-1 (Fer) suppressed the expression of Nrf2 target genes induced by ox-LDL (Fig. 2K). In addition, oscillatory shear stress, another critical atherogenic factor (OSS, 4 dyne/cm^2, 16 h) also increased the expression of Nrf2 and its target genes, such as *HMOX1*, *TXNRD1*, *SLC3A2*, *SLC7A11* in HUVECs (Supplemental F ig. 3C-3F). Taken together, these results reveal that endothelial inflammation and LPO were among the earliest events after HCD feeding in *ApoE*$^{-/-}$ mice, which consequently induced Nrf2 activation (Fig. 2L). However, the detailed role of Nrf2 activation in ECs is unclear.

3.3. Inhibition of Nrf2 increased endothelial lipid peroxidation and inflammation

To investigate the role of Nrf2 in endothelial inflammation and LPO, we silenced Nrf2 in HUVECs by shRNA and performed RNA sequencing analysis. The efficacy of the knockdown was verified by the Western blot method (Supplemental Fi gure 4A). The KEGG enrichment analysis revealed that the most enriched pathways were related to chemokines, NF-κB, pattern recognition receptors (e.g., NOD-like receptor, RIG-like receptor, and Toll-like receptors), glutathione metabolism, and ferroptosis (Fig. 3A). The GSEA enrichment analysis further revealed that Nrf2 knockdown was positively associated with an endothelial inflammatory response while it was negatively related to the expression of glutathione metabolism-related genes (Fig. 3B & 3C). Consistently, Nrf2 knockdown increased ROS production in ECs (Supplemental F ig. 4B&4C), supporting the crucial role of Nrf2 in redox homeostasis and inflammation. Liperfluo staining showed that Nrf2 knockdown exacerbated LPO in HUVECs after exposure to H_2O_2 (100 μM, 3 h) or TNF-α (10 ng/mL, 12 h) (Fig. 3D–3F). In the presence of TNF-α, deferoxamine (DFO, 100 μM) reversed LPO induced by Nrf2 knockdown (Fig. 3G). In addition, Nrf2 knockdown increased TNF-α-induced expression of inflammatory (*TNFA*) and adhesion molecules (*VCAM1*, *SELE*) (Supplemental F ig. 4D&4E) and DFO inhibited shNrf2-induced mRNA expression of *VCAM1*, *TNFA*, and *IL1B* (Fig. 3G), as well as the attachment of monocytes to HUVECs (Fig. 3H&3I). Brusatol, a Nrf2 and general protein synthesis inhibitor, suppressed Nrf2 expression in a time- and concentration-dependent manner (Supplemental Fi gure 5A). Moreover, treatment with brusatol (100 nM, 12 h) resulted in a marked increase in LPO in HAECs (Supplemental F ig. 5B&5C). In addition, brusatol upregulated the expression of *VCAM1*, *SELE*, *CCL2*, *TNFA*, and *IL1B* in both control and TNF-α-treated HUVECs (Supplemental Fi g. 5D&5E). These findings suggest that Nrf2 deficiency exacerbates endothelial inflammation and LPO induced by atherogenic risk factors.

3.4. Endothelial Nrf2 knockdown accelerated atherosclerosis

To investigate whether endothelial Nrf2 deficiency promotes atherogenesis, we generated *Cdh5*^{Cre}*Cas9*$^{floxed\text{-}stop}$*ApoE*$^{-/-}$ mice by crossbreeding *Cdh5*^{Cre}*Cas9*$^{floxed\text{-}stop}$*with ApoE*$^{-/-}$ mice (Supplemental Fi gure 6A). Successful expression of Cas9 in vascular ECs was confirmed by Western blotting (Supplemental Fi gure 6B). To achieve specific Nrf2 knockdown in endothelial cells, we administered AAV-U6-sgRNA targeting Nrf2 (*Nrf2*^{ecKD}) or empty vector (control) to *Cdh5*^{Cre}*Cas9*$^{floxed\text{-}stop}$*ApoE*$^{-/-}$ mice via tail vein injection. We validated the knockdown efficacy of Nrf2 sgRNAs *in vitro* using the Cas9 expressing Hepa1-6 cell line (Supplemental Fi gure 6C). Three weeks after AAV injection, the mice were fed with HCD for eight weeks to induce plaque formation. The protein levels of Nrf2, as well as the downstream NQO1 and heme oxygenase-1 (HO-1) were reduced in lung ECs isolated from *Nrf2*^{ecKD} mice (Supplemental Fi g. 6D&6E). Immunofluorescent staining further confirmed the successful knockdown of Nrf2 in ECs of mouse aortas (Supplemental F igure 6F). Oil red O staining revealed that *Nrf2*^{ecKD} mice developed more atherosclerotic plaques in their aortas and aortic roots than vector control mice (Fig. 4A–4D). However, the plasma lipid levels did not differ between the two groups (Supplemental F igure 6G). This indicates that the atherogenesis-enhancing effect of endothelial Nrf2 knockdown is independent of lipid profiles. Higher levels of VCAM-1 and 4-HNE staining were detected in the endothelial and medial layers of the aortas with lesions in *Nrf2*^{ecKD} mice, indicating increased endothelial inflammation and LPO (Fig. 4E–4G). These results demonstrate that *in vivo* knockdown of endothelial Nrf2 enhances endothelial inflammation and LPO, promoting HCD-induced atherogenesis in *ApoE*$^{-/-}$ mice.

3.5. Endothelial Nrf2 activation inhibited inflammation, lipid peroxidation, and atherosclerosis

To demonstrate the critical role of Nrf2 in endothelial inflammation and LPO, we activated Nrf2 in HUVECs by knocking down Keap1 using lentivirus (Supplemental Fi gure 7A). Both qPCR and Western blot results showed that Keap1 knockdown attenuated TNF-α-induced

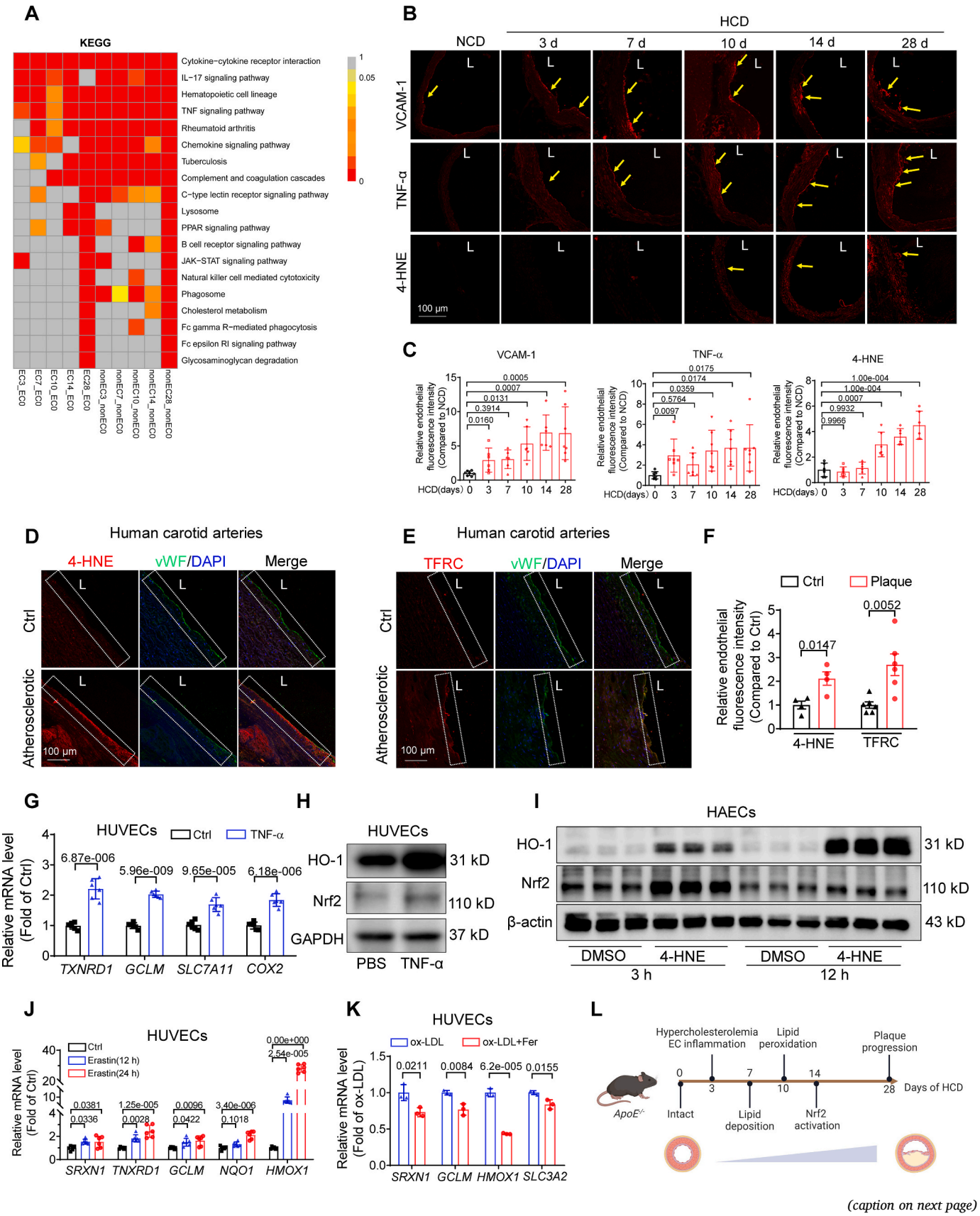

(caption on next page)

Fig. 2. Endothelial inflammation and lipid peroxidation contributed to Nrf2 activation during atherogenesis.
(A) The KEGG analysis results revealed the enriched signaling pathways of the aortic EC and non-EC components in *ApoE*$^{-/-}$ mice after being fed with an HCD for 3, 7, 10, 14, and 28 days. (B) Representative immunofluorescence images of VCAM-1, TNF-α and 4-HNE in the aortas of *ApoE*$^{-/-}$ mice. The yellow arrowhead denotes VCAM-1 (+), TNF-α (+) and 4-HNE (+) ECs in aortas. (C) Statistical analysis results for (B). (D & E) Representative immunofluorescence images of 4-HNE (red) and TFRC (red) in the carotid arteries of human atherosclerotic lesions. vWF (green) is an EC marker. (F) Statistical analysis results for (D & E). (G & H) HUVECs were exposed to 10 ng/mL TNF-α for 12 h, the expression of Nrf2 and target genes were measured using Western blot and qPCR. (I) HAECs were incubated with 50 μM 4-HNE for the indicated time, western blotting was used to determine the protein levels of Nrf2 and HO-1. (J) HUVECs were treated with erastin (20 μM) and the mRNA levels of Nrf2 targeted genes were detected by qPCR, n = 4–6. (K) HUVECs were pretreated with Fer (2 μM) for 0.5 h before being exposed to 75 μg/mL ox-LDL for 12 h, the mRNA levels of Nrf2 target genes were measured using qPCR, n = 4. (L) The schematic model illustrates the timing of EC inflammation, LPO, and Nrf2 activation. Results are means ± SD. Statistical analysis was performed using an unpaired two-tailed Student's *t*-test for (F), (G) and (K) and a one-way ANOVA followed by Tukey's test for (C) and (J). L, lumen. (For interpretation of the references to color in this figure legend, the reader is referred to the Web version of this article.)

expression of *TNFA*, *VCAM1* and *SELE* (Fig. 5A&5B; Supplemental F igure 8) and monocyte adhesion to HUVECs (Fig. 5C& 5D). Likewise, ox-LDL-induced LPO was also reduced in Keap1-knocked down HUVECs (Fig. 5E &5F). To further validate the involvement of endothelial Nrf2 in atherogenesis, we activated endothelial Nrf2 in *ApoE*$^{-/-}$ mice by administering an EC-specific AAV9 encoding saCas9 and Keap1 sgRNA. We isolated lung ECs to verify the knockdown efficacy of sgKeap1. The protein levels of Nrf2 and its targeted genes NQO1 and HMOX1 were markedly elevated after Keap1 knockdown, which was further confirmed by the immunostaining in mouse aortas (Supplemental F ig. 7B-7D). EC-specific knockdown of Keap1 reduced the plaque area in aortas of male and female *ApoE*$^{-/-}$ mice, thus supporting the athero-protective effect of endothelial Nrf2 (Fig. 5G–5J). The expression of 4-HNE and VCAM-1 in intima and medial layers of aortas from *ApoE*$^{-/-}$ mice was also decreased (Fig. 5K&5L), supporting that Nrf2 activation inhibits endothelial inflammation and LPO, leading to an anti-atherogenic effect. However, endothelial Keap1 knockdown mice had higher plasma levels of LDL cholesterol and a rise in total cholesterol levels, whereas plasma triglyceride and HDL cholesterol concentrations or body weight remained unchanged (Supplemental F ig. 7E&7F). This is likely to be explained by the effects of Nrf2 in the induction of the scavenger receptor CD36 in ECs [35]. Ox-LDL and high fat diet feeding can upregulate endothelial CD36, which promotes the uptake of ox-LDL and fatty acids that are also involved in systemic glucose metabolism and lipid metabolism. Despite the fact of the increased LDL levels, EC-specific Nrf2 activation resulted in a significant athero-protective effect, further indicating the anti-inflammatory and anti-oxidative effects of endothelial Nrf2 are likely to outweigh the potential negative impact of increased LDL cholesterol on atherogenesis. Overall, these results demonstrate that the activation of endothelial Nrf2 is a secondary response to the initial induction of the inflammation-LPO axis. It is likely to function as a compensatory mechanism that restrains further endothelial inflammation and LPO, thereby limiting the progression of atherosclerosis.

3.6. Dimethyl itaconate (DMI), an Nrf2 activator, inhibited endothelial inflammation

Previous studies have reported that itaconate and fumarate are two intrinsic electrophiles that activate Nrf2 by alkylating the cysteine-SH of Keap1 in macrophages [36]. To investigate whether DMI activates Nrf2 in ECs, we profiled the mRNA expression of HUVECs following a 15 h-treatment with DMI (100 μM). The KEGG enrichment analysis showed enrichment in pathways related to glutathione metabolism, ferroptosis, fluid shear stress, and atherosclerosis (Supplemental F igure 9A). The data from the heatmap showed that DMI induced the expression of many Nrf2 target genes (Fig. 6A) and the Western blotting results demonstrated that DMI activated Nrf2 signaling pathway in a time-dependent manner (Fig. 6B and Supplemental Fi g. 9B&9C&9D). Nrf2 and its target proteins such as HO-1 and P62 were significantly upregulated from 3 h to 24 h. Treatment with DMI (100 μM) or dimethyl fumarate (DMF, 100 μM) for 6 h resulted in increased protein expression of Nrf2 in both the nucleus and cytosol fractions (Supplemental F ig. 9E&9F). The qPCR results showed that DMI inhibited the expression of *VCAM1* and *TNFA* induced by TNF-α (10 ng/mL, 12 h) (Supplemental Fi gure 10A). DMI also inhibited TNF-α-induced attachment of THP-1 monocytes to HUVECs (Supplemental Fi g.10B&10C). Furthermore, DMI produced a similar anti-inflammatory effect in HUVECs exposed to IL-1β (10 ng/mL) or LPS (100 ng/mL) (Supplemental Fi g. 10D-10G). NF-κB is crucial in the regulation of inflammation. RNA-seq data indicated that DMI inhibited most of TNF-α-induced transcription of inflammatory and adhesion genes which are regulated by NF-κB (Supplemental F igure 11A). Interestingly, DMI did not inhibit either canonical or non-canonical NF-κB pathway (Supplemental F ig. 11B&11C). The results from the dual luciferase assay of NF-κB transcriptional activity (Supplemental F igure 11D) further support this, indicating that the anti-inflammatory effect of DMI is not related to NF-κB inhibition. To explore whether the action of DMI was mediated through Nrf2 activation, we created a Nrf2 knockdown HUVEC line using lentivirus-mediated gene interference. Both SCR and Nrf2 knockdown HUVECs were pretreated with DMI (100 μM, 3 h) followed by a 12-h incubation with TNF-α (10 ng/mL). The Western blotting results showed that Nrf2 knockdown significantly reduced the inhibitory effect of DMI on the VCAM-1 expression (Fig. 6C&6D). To investigate how DMI activates Nrf2, we incubated HUVECs with DMI and measured the electrophilic and oxidation states after treatment for 1, 3, and 12 h. Within 1 h, DMI caused a significant decrease in glutathione (GSH) levels (Fig. 6E) and an increase in oxidized GSH (GSSG) levels (Fig. 6F). However, after 12 h of DMI treatment, the ROS level was found to decrease, as indicated by DCFDA staining (Fig. 6G). These findings suggest that DMI induces rapid electrophilic stress, which may contribute to the long-term reduction of oxidative stress. To investigate whether electrophilic stress mediates DMI-induced Nrf2 activation, we treated HUVECs with N-acetyl-L-cysteine (NAC) and GSH, both of which are electrophilic stress suppressors, for 3 h, followed by DMI for 12 h. The results showed that NAC (1 mM) and GSH (2 mM) inhibited DMI-induced Nrf2 activation and HO-1 expression (Fig. 6H&6J). Furthermore, the inhibitory effect of DMI (100 μM, 15 h) on TNF-α (10 ng/mL, 12 h)-induced inflammation was reversed by NAC and GSH (Fig. 6I&6J). This supports the idea that DMI-induced electrophilic stress is most likely to mediate its anti-inflammatory effect by activating Nrf2 in ECs. However, the direct connection of reductive stress to Nrf2 activation has to be further investigated.

3.7. DMI inhibited the initiation of atherosclerosis in *ApoE*$^{-/-}$ mice

To determine whether DMI activates endothelial Nrf2 *in vivo*, we orally administered *ApoE*$^{-/-}$ mice with DMI (100 mg/kg) for 6 h, and isolated both aortic ECs and non-ECs for qPCR. *Cdh5* and *Cnn1* were used to confirm the purification efficacy of ECs (Supplemental F ig. 12A&12B). The results showed that DMI increased the expression of Nrf2 target genes (*Gclm*, *Gclc*, *Hmox1*, and *Slc7a11*) and suppressed the expression of inflammatory molecules (*Tnfa* and *Sele*) in the aortic ECs of *ApoE*$^{-/-}$ mice (Supplemental Fi gure 12C). To investigate whether activation of Nrf2 in *ApoE*$^{-/-}$ mice has a protective effect against atherosclerosis, 10-week-old *ApoE*$^{-/-}$ mice were fed with HCD for 4

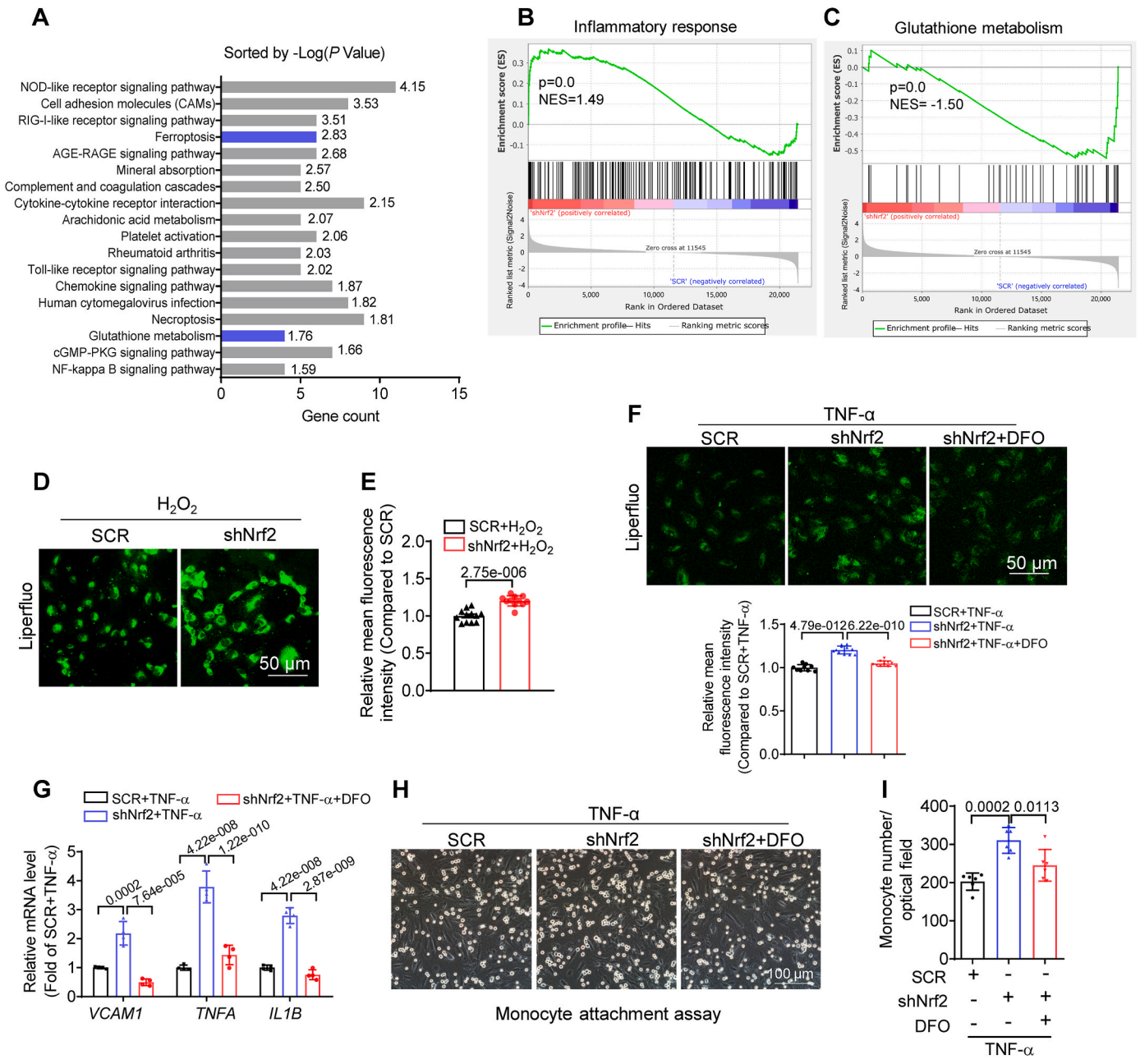

Fig. 3. Knockdown Nrf2 increased lipid peroxidation and inflammation in endothelial cells.
HUVECs were infected with lentivirus encoding Nrf2 shRNA and underwent RNA sequencing. (A) KEGG enrichment analysis revealed alterations in signaling pathways. GSEA was used to analyze the changes in the inflammatory response (B) and glutathione metabolism (C) pathways. (D) SCR and shNrf2-treated HUVECs were incubated with ox-LDL (75 μg/mL) for 36 h or H_2O_2 (100 μM) for 3 h. The liperfluo staining was used to measure the lipid peroxidation state. (E) Statistical analysis result for (D), n = 8–12. (F) SCR and shNrf2-treated HUVECs were pretreated with DFO (100 μM) for 0.5 h and then incubated with TNF-α (10 ng/mL) for 12 h. The representative images and statistical summary of liperfluo staining are shown, n = 9–11. (G) SCR- and shNrf2-treated HUVECs were pretreated with deferoxamine (DFO, 100 μM) for 0.5 h and then incubated with TNF-α (10 ng/mL) for 12 h. The mRNA expression of inflammatory genes was measured using qPCR, n = 4. (H) The THP1 monocyte adhesion to HUVECs, n = 6. (I) Statistical analysis for (H). Results are means ± SD. Statistical analysis was performed using an unpaired two-tailed Student's *t*-test for (E) and a one-way ANOVA followed by Tukey's test for (F), (G), and (I).

weeks. During this period, DMI was administered either from week 1 (prevention group) or week 3 (treatment group) until the end of the experiment (Fig. 7A). Immunostaining revealed a significant increase in endothelial Nrf2 expression following DMI treatment (Supplemental F ig. 12D&12E). Oil red O staining showed that DMI can both prevent and attenuate HCD-induced atherosclerosis (Fig. 7B&7C). This anti-atherogenic effect of DMI was reduced in EC-specific Keap1 knock-down mice with constitutive activation of the Nrf2 pathway (Fig. 5G–5J), further supporting that the athero-protective effect of DMI is due to the activation of endothelial Nrf2. Body weight, triglyceride, total cholesterol, HDL, and LDL remained unchanged (Supplemental F ig. 12F&12G). In addition, in accordance with the total plaque area, staining for VCAM-1 and 4-HNE (Fig. 7D–7F) showed that DMI reduced endothelial inflammation and LPO in the ascending aortas. The present results demonstrate that pharmacological activation of Nrf2 with DMI is effective in inhibiting the initiation of atherosclerosis and reversing atherogenesis in *ApoE*$^{-/-}$ mice.

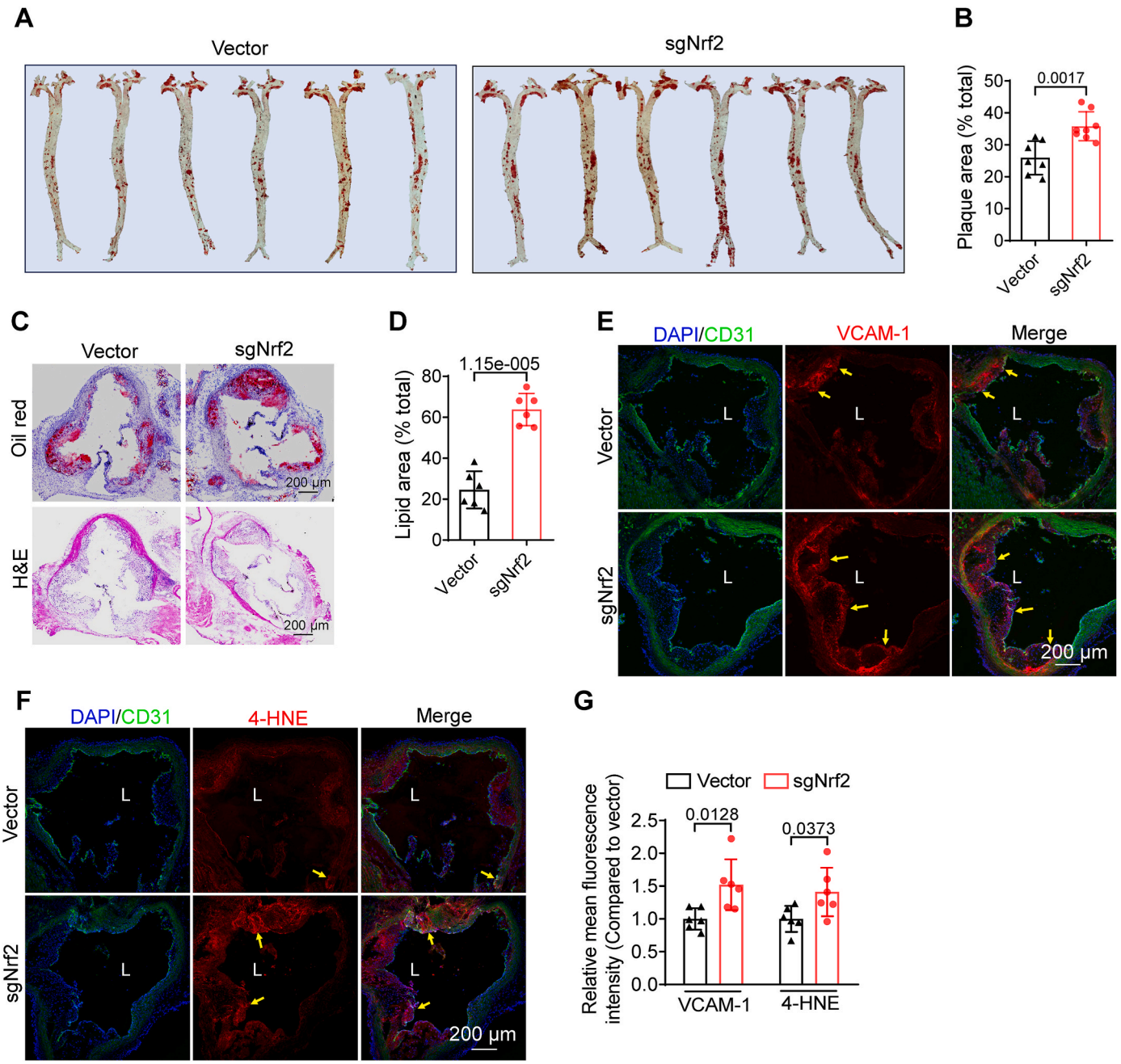

Fig. 4. Endothelium-specific knockdown Nrf2 exacerbated atherosclerosis.
Cdh5^{Cre}*Cas9*$^{floxed\text{-}stop}$*ApoE*$^{-/-}$ mice were injected with AAV9-sgNrf2 via tail veins and maintained for 3 weeks followed by 8 weeks of HCD feeding. (A) Representative images and (B) statistical analysis of the atherosclerotic plaque stained by Oil Red O staining. n = 6–8. (C & D) The lesions of the aortic root were stained by Oil Red O staining and H&E staining. Immunofluorescence images (E & F) and statistical summary (G) of VCAM-1 and 4-HNE staining in aortas, n = 6–8. Results are means ± SD. Statistical analysis was performed using an unpaired two-tailed Student's *t*-test for (B), (D) and (G). L, lumen. (For interpretation of the references to color in this figure legend, the reader is referred to the Web version of this article.)

4. Discussion

Nrf2 is a transcription factor that is activated by stress and plays a crucial role in modulating oxidative stress and inflammatory responses among other cellular processes [13]. Previous studies have shown that the role of Nrf2 in regulating atherosclerosis pathogenesis varies across different cell types. For instance, in bone marrow cells, Nrf2 facilitates the formation of foam cells by increasing CD36 expression, thereby accelerating atherosclerosis [35]. In aortic SMCs, Nrf2 was reported before to be adaptively activated in response to a wide range of stressors, including oxidized LDL and inflammatory cytokines [37]. This activation helps maintain cellular redox homeostasis and promotes a youthful cellular phenotype by regulating the transcription of an array of cytoprotective genes. However, dysfunction of Nrf2 can lead to impaired cellular resistance to oxidative stressors, contributing to the development of age-related vascular disorders including atherosclerosis [37]. Recent studies have also highlighted the role of Nrf2 in connecting autophagy and vascular senescence in atherosclerosis [38,39]. In endothelial cells, Nrf2 inhibits the inflammatory response and oxidative stress, which are two key mechanisms for the initiation of atherosclerosis, suggesting that the beneficial effect of Nrf2 in endothelial cells might outweigh other cell types in the vasculature. Although endothelial

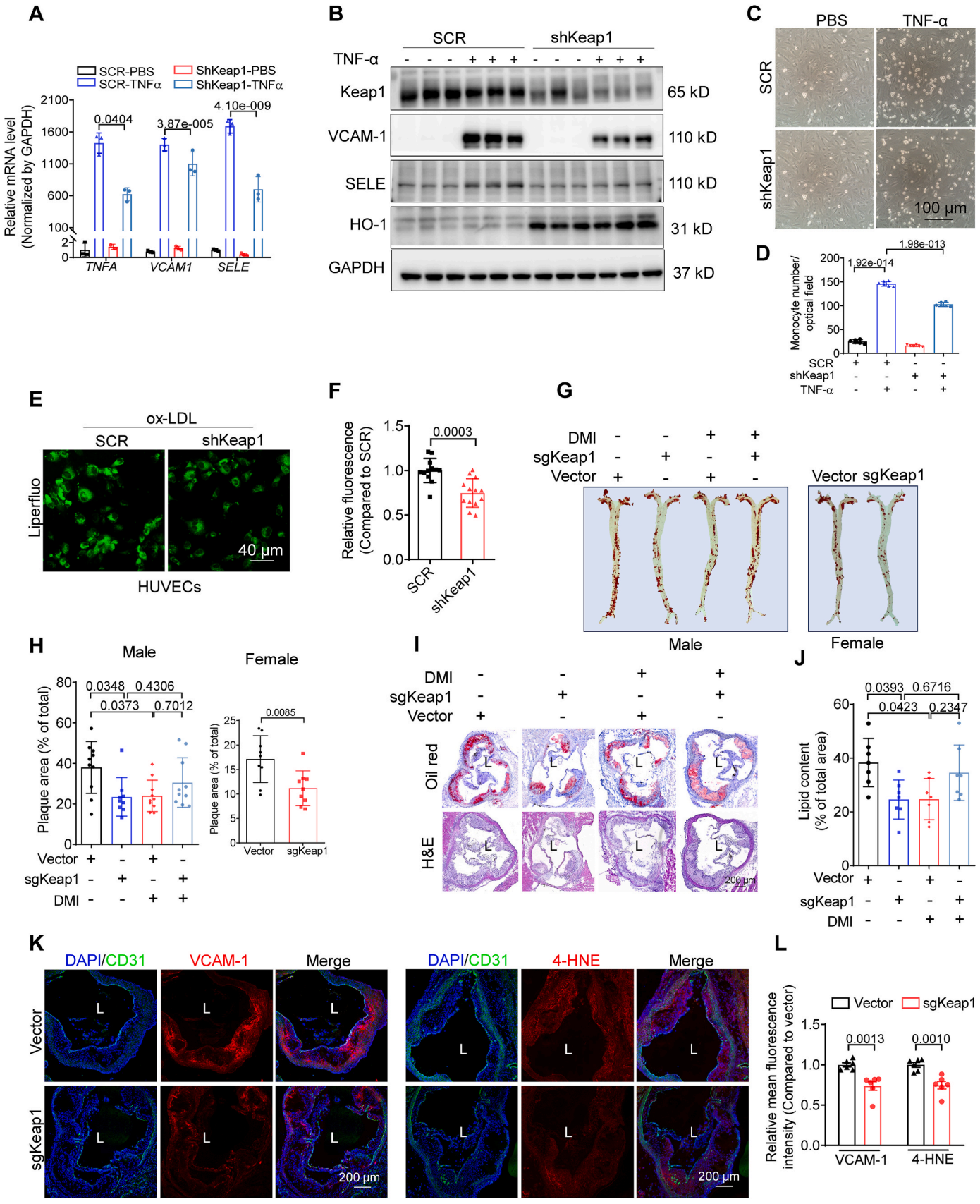

(caption on next page)

Fig. 5. Endothelium-specific activation of Nrf2 inhibited lipid peroxidation, inflammation and atherosclerosis.
SCR- and shKeap1-infected HUVECs were incubated with TNF-α (10 ng/mL) for 12 h. (A) the mRNA levels of *TNFA*, *VCAM1*, and *SELE*, (B) the protein levels of VCAM-1, SELE, HO-1, NQO1, and Keap1 were measured. (C, D) SCR- and shKeap1-treated HUVECs were incubated with TNF-α (10 ng/mL) for 12 h; the THP1 monocyte adhesion to HUVECs was measured, n = 6. (E) SCR- and shKeap1-treated HUVECs were incubated with ox-LDL (75 μg/mL) for 36 h, liperfluo fluorescence intensity was measured by confocal microscopy, n = 11–12. (F) The summary statistical result for (E). Male and female *ApoE*$^{-/-}$ mice were injected with AAV9-CMV-Cas9-U6-sgKeap1 via tail veins for 3 weeks, followed by 8 weeks of HCD feeding. (G) Representative images and (H) statistical analysis result of the atherosclerotic plaque stained by Oil Red O staining, n = 10. (I, J) The Oil Red O staining and H&E staining were performed to measure the aortic root lesions. Immunofluorescence images (K) and the statistical analysis result (L) of VCAM-1 and 4-HNE staining in aortas of *ApoE*$^{-/-}$ mice, n = 6. Results are means ± SD. Statistical analysis was performed using two-way repeated measures ANOVA followed by Tukey's test for (A), (D), (H) and (J), unpaired two-tailed Student's *t*-test for (F) and (L). L, lumen. (For interpretation of the references to color in this figure legend, the reader is referred to the Web version of this article.)

Nrf2 is vaso-protective, direct evidence for its role against atherosclerosis is lacking.

To explain how endothelial Nrf2 was activated during atherogenesis, we performed RNA sequencing analyses on ECs and non-ECs of aortas from *ApoE*$^{-/-}$ mice after different durations of HCD feeding. Notably, endothelial inflammatory responses appeared as early as on day 3 post-HCD, as evidenced by KEGG, GSEA, and WGCNA enrichment analyses and immunofluorescence staining. In contrast, endothelial LPO began to increase on day 10, subsequent to earlier endothelial inflammation. The obvious upregulation of Nrf2 target genes in mouse aortic ECs only between days 10 and 14, after the onset of inflammation and LPO, suggests a potential causal relationship with Nrf2 activation. This likelihood is further supported by the observation that treatment with TNF-α, 4-HNE, erastin and Fer increased the expression of Nrf2 target genes in human ECs. The present results highlight the dual roles of EC inflammation and LPO both in promoting atherogenesis and in activating Nrf2 to limiting these harmful effects and thus retarding atherosclerotic progression.

Previous studies reported that treatment with low doses of 4-HNE and oxidized phospholipids can induce the expression of antioxidant and detoxifying genes via Nrf2 activation in HeLa cells and human endothelial cells [40,41]. The present study shows that Nrf2 is most likely to mediate the anti-inflammatory effect of LPO based on the following observations. First, treatment with erastin, an LPO inducer, activates Nrf2 signaling in HUVECs. In addition, TNF-α, ox-LDL and OSS, which are shown to induce LPO, can also activate Nrf2 in HUVECs and HAECs. Second, to confirm whether Nrf2 plays a significant role in regulating endothelial inflammation, we performed RNA-seq, qPCR, and western blotting analysis and demonstrated that Nrf2 knockdown augmented TNF-α-induced endothelial inflammation, which was reversed by LPO inhibitors. Treatment with Nrf2 inhibitor (brusatol) increased inflammation and LPO in human endothelial cells in the absence and presence of TNF-α. Third, EC-specific Nrf2 knockdown accelerated plaque formation, accompanied by elevated expression of VCAM-1 and 4-HNE in vascular endothelium. Oppositely, EC-specific activation of Nrf2 by knocking down Keap1 reduced inflammation and LPO, and thus retarded atherogenesis. Finally, increased Nrf2 expression was detected in the endothelial layer of human aortas with intimal thickening. The above evidence indicates that endothelial Nrf2 can be activated by inflammation and LPO, which serves as a negative feedback mechanism to mitigate further endothelial inflammation and LPO, thereby decelerating progression of atherosclerosis in *ApoE*$^{-/-}$ mice.

Apparently, the observation of decreased atherosclerosis and increased levels of blood total cholesterol and LDL in response to endothelial-specific Keap1 knockdown is of significant interest in the context of atherogenesis. Previous studies suggest that Nrf2 increases the expression of scavenger receptor class A (SR-A) and CD36 (for cholesterol influx) as well as ABCA1 and ABCG1 (for cholesterol efflux) [42,43], which might partially explain the elevation in total cholesterol and LDL observed in our study. However, the activation of Nrf2 resulting from Keap1 knockdown enhances the antioxidant and anti-inflammatory capacity of endothelial cells, which may override the potential adverse impact of elevated cholesterol and LDL, and thus providing overall vaso-protection. This may also underscore the multi-faceted roles of the Keap1-Nrf2 signaling during atherogenesis. Combined therapies targeting both Nrf2 and cholesterol pathways may produce better outcomes in the treatment of atherosclerotic vascular disease.

Previous studies have suggested the discrepancy for the roles of Nrf2 in hematopoietic cells in atherosclerosis in *ApoE*$^{-/-}$ and *LDLR*$^{-/-}$ mice requires further analysis, especially in consideration of the different metabolic and cellular pathways in these two genetic mouse models. First of all, *ApoE*$^{-/-}$ mice typically exhibit severe hypercholesterolemia with increased levels of very low-density lipoproteins (VLDL) and chylomicron remnants due to a failure in lipoprotein clearance, while *LDLR*$^{-/-}$ mice primarily have elevated levels of LDL due to reduced clearance of LDL particles, the latter probably mimics human familial hypercholesterolemia more closely [44]. In *ApoE*$^{-/-}$ mice, the lack of apoE affects not only lipid metabolism but also immune modulation, as ApoE plays roles in immune regulation, which could affect the inflammatory response during atherogenesis independently of lipid levels [44,45]. By contrast, *LDLR*$^{-/-}$ mice lack these direct immunomodulatory effects that are driven by apoE deficiency, making this atherosclerotic model more specific to disruption in lipid handling. The discrepancy in the impact of Nrf2 on atherosclerosis between *ApoE*$^{-/-}$ and *LDLR*$^{-/-}$ models might arise from different baseline inflammatory levels and oxidative environments due to their distinct lipid profiles and lipoprotein functionalities in the two mouse models [45]. Further investigation is needed to understand the role of macrophage Nrf2 in atherogenesis in these two mouse models of atherosclerosis. As endothelial dysfunction is known to be an early triggering event during atherogenesis, we tend to anticipate that Nrf2 activation in vascular endothelial cells shall result in suppressive effects on endothelial inflammation and plaque formation in both *ApoE*$^{-/-}$ and *LDLR*$^{-/-}$ mice, regardless the cause of dyslipidemia. The vaso-protective effects of Nrf2 activation are likely to be a universal benefit through reducing oxidative damage and inflammation.

Itaconate and its esterified derivative DMI are electrophiles that are previously described to activate Nrf2 in macrophages [36,46,47]. DMI has been shown to protect against psoriasis [48] and LPS lethality [36] in rodent models. Our results demonstrate that DMI effectively inhibits inflammation in human endothelial cells. Although NF-κB is a master regulator of inflammation, DMI does not inhibit the canonical or non-canonical NF-κB pathway. However, Nrf2 knockdown can reverse the anti-inflammatory effect of DMI, indicating that Nrf2 is a major target of DMI action. Furthermore, *in vivo* administration of DMI to *ApoE*$^{-/-}$ mice resulted in reduced plaque formation, endothelial inflammation and LPO; this was accompanied by endothelial Nrf2 activation in the aortas. More importantly, DMI has a reduced effect on plaque formation in *ApoE*$^{-/-}$ mice with EC-specific Nrf2 activation. This suggests that the athero-protective effect of DMI is likely due to activation of endothelial Nrf2. DMI-induced pharmacological activation of Nrf2 is effective in inhibiting both the initiation and progression of atherosclerosis in *ApoE*$^{-/-}$ mice.

Summary

The present study demonstrates that EC inflammation occurs within 3 days after HCD feeding, followed by the appearance of LPO around day 10. Inflammatory factors and LPO end-products then activate Nrf2 to limit further endothelial inflammation and LPO, thereby retarding the

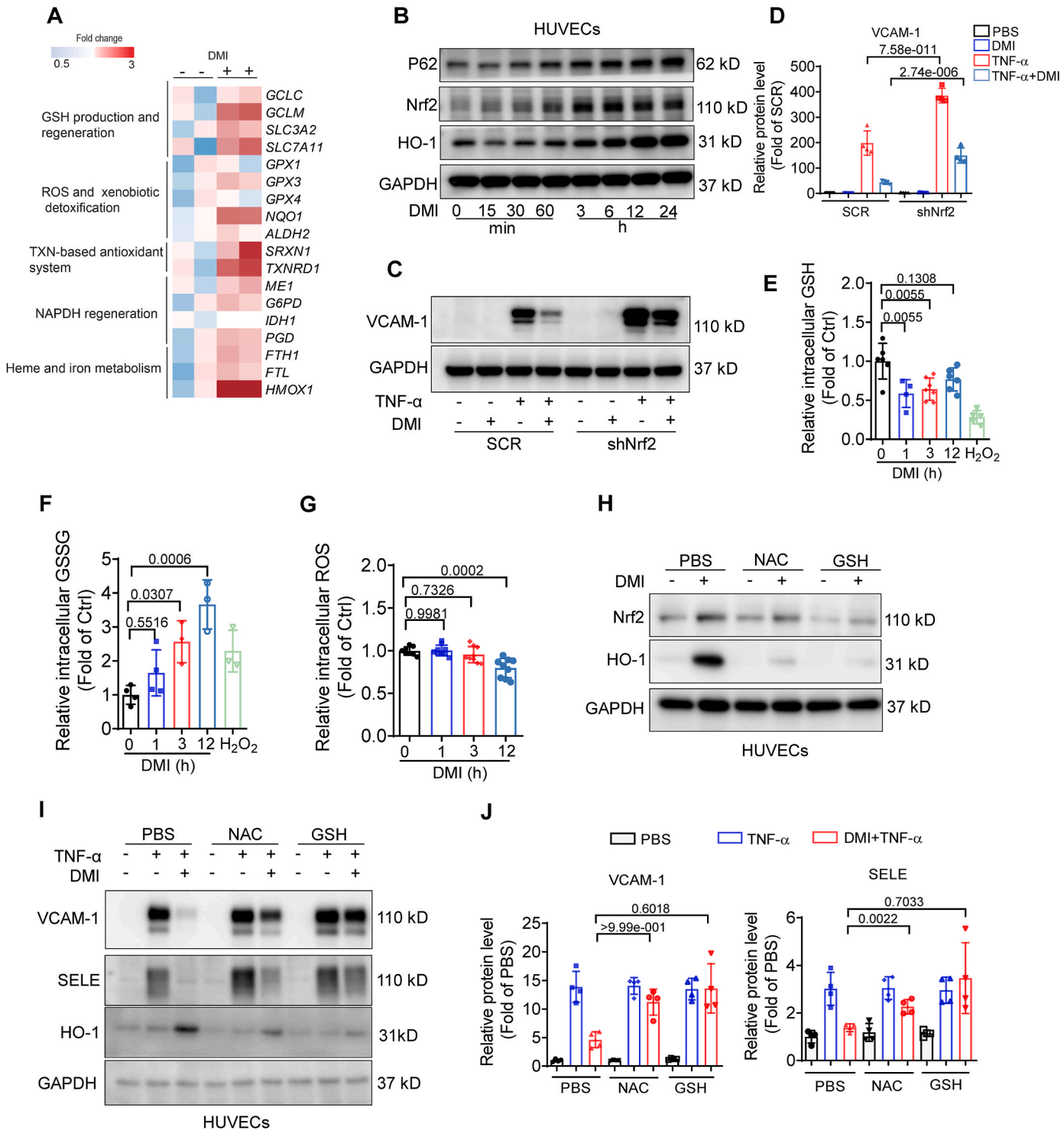

Fig. 6. Dimethyl itaconate (DMI) suppressed endothelial inflammation through activating Nrf2.
HUVECs were incubated with DMI (100 μM) for 15 h for RNA sequencing. (A) A heatmap of Nrf2 target genes was generated. (B) HUVECs were incubated with DMI for different time points to measure the protein levels of p62, Nrf2, and HO-1. (C, D) SCR and Nrf2 knockdown HUVECs were pretreated with DMI (100 μM, 3 h) followed by incubation with TNF-α (10 ng/mL) for 12 h, protein level of VCAM-1 was measured using Western blotting, n = 4. HUVECs were incubated with DMI (100 μM) for 1, 3, and 12 h H_2O_2 (100 μM, 1 h) was used as a positive control. The levels of GSH (E) and GSSG (F) were determined (n = 4–7). (G) Reactive oxygen species levels were measured by flow cytometry analysis after CM-H2DCFDA staining of HUVECs following treatment with DMI for 1, 3, and 12 h n = 9. (H) HUVECs were pretreated with DMI (100 μM) for 3 h followed by NAC (1 mM) and GSH (2 mM) for 12 h. The protein levels of Nrf2 and HO-1 were measured. (I) HUVECs were pretreated with DMI (100 μM) for 3 h followed by NAC (1 mM) and GSH (2 mM) in the presence of TNF-α (10 ng/mL) for 12 h; the protein levels of VCAM-1, SELE and HO-1 were measured. (J) Statistical summary of (I), n = 4. Treatment medium, DMEM (0.5 mM glucose, without pyruvate or glutamine). NAC, N-acetyl cysteine; GSH, glutathione. Results are means ± SD. Statistical analysis was performed using One-way ANOVA followed by Tukey's test for (D), (E–G) and (J).

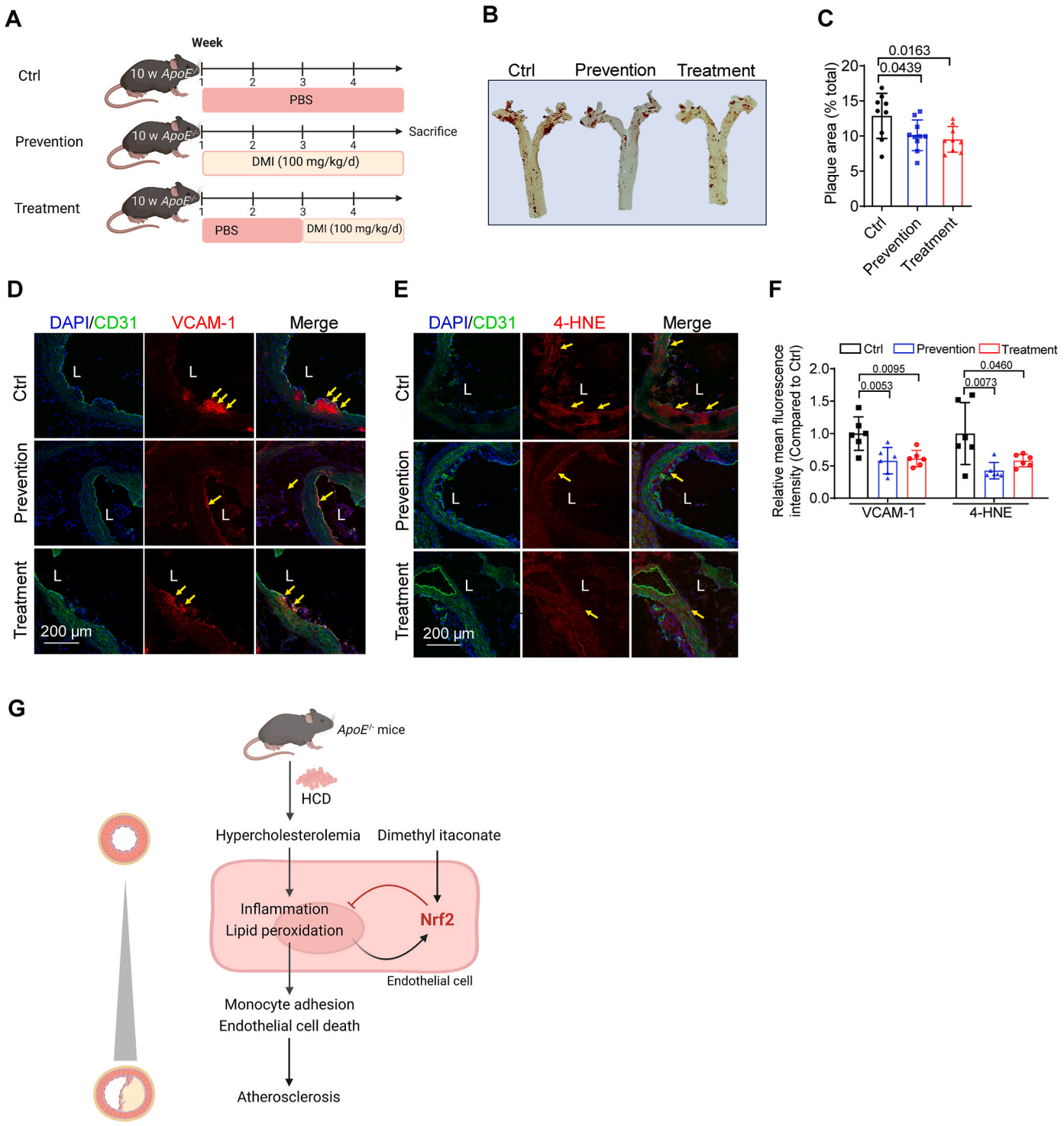

Fig. 7. DMI inhibited atherosclerosis in *ApoE*−/− mice. (A) The protocol of DMI administration to *ApoE*$^{-/-}$ mice. The prevention group received HCD for 4 weeks with daily DMI administration, while the treatment group received HCD for 4 weeks with daily DMI administration during the last 2 weeks. (B, C) After the 4-week treatment, plaque formation was measured in the aortas, aortic arch and descending thoracic aortas using Oil Red O staining, n = 9–10. (D, E) Representative immunofluorescence images and (F) statistical summary of VCAM-1 and 4-HNE staining in aortas of *ApoE*$^{-/-}$ mice, n = 6. (G) A schematic diagram illustrates the sequential roles of inflammation, LPO and Nrf2 in atherogenesis. Results are means ± SD. Statistical analysis was performed using One-way ANOVA followed by Tukey's test for (C) and (F). The yellow arrowhead indicates VCAM-1 (+) or 4-HNE (+) cells in the aortic plaque. L, lumen. (For interpretation of the references to color in this figure legend, the reader is referred to the Web version of this article.)

progression of atherosclerosis (Fig. 7G). Strategies aimed to activate endothelial Nrf2 may be a potentially promising approach for the prevention and early intervention in atherosclerotic vascular diseases.

Sources of funding

This study was supported by Hong Kong Research Grants Council (T12-101/23-N, SRFS2021-4S04, 14109720, 14100121), HMRF

(07181286), and Natural Science Foundation of China (91939302, 82370259).

CRediT authorship contribution statement

Lei He: Writing – review & editing, Writing – original draft, Validation, Methodology, Data curation, Conceptualization. **Qinghua Chen:** Methodology, Data curation. **Li Wang:** Methodology, Data curation. **Yujie Pu:** Methodology. **Juan Huang:** Methodology. **Chak Kwong Cheng:** Methodology. **Jiang-Yun Luo:** Methodology. **Lijing Kang:** Methodology. **Xiao Lin:** Methodology. **Li Xiang:** Methodology. **Liang Fang:** Methodology. **Ben He:** Methodology. **Yin Xia:** Supervision. **Kathy O. Lui:** Supervision. **Yong Pan:** Supervision. **Jie Liu:** Supervision. **Cheng-Lin Zhang:** Writing – review & editing, Supervision, Funding acquisition, Data curation, Conceptualization. **Yu Huang:** Writing – review & editing, Supervision, Project administration, Funding acquisition.

Declaration of competing interest

The authors declare that there is no conflict of interest regarding the publication of this paper.

Data availability

Data will be made available on request.

Acknowledgement

We thank Mr. Chi Wai Lau (Chinese University of Hong Kong) for assistance on animal experiments. We thank Professor Ai-Jun Sun from Fudan University for providing advice on this project. All schematic diagrams are prepared using BioRender web-based software.

Appendix ASupplementary data

Supplementary data to this article can be found online at https://doi.org/10.1016/j.redox.2024.103229.

References

[1] P. Libby, The changing landscape of atherosclerosis, Nature 592 (2021) 524–533.
[2] P. Libby, P. Theroux, Pathophysiology of coronary artery disease, Circulation 111 (2005) 3481–3488.
[3] P.M. Ridker, B.M. Everett, T. Thuren, J.G. MacFadyen, W.H. Chang, C. Ballantyne, et al., Antiinflammatory therapy with canakinumab for atherosclerotic disease, N. Engl. J. Med. 377 (2017) 1119–1131.
[4] P. Libby, B.M. Everett, Novel antiatherosclerotic therapies, Arterioscler. Thromb. Vasc. Biol. 39 (2019) 538–545.
[5] P.M. Ridker, M. Rane, Interleukin-6 signaling and anti-interleukin-6 therapeutics in cardiovascular disease, Circ. Res. 128 (2021) 1728–1746.
[6] E. Gianazza, M. Brioschi, A. Martinez Fernandez, F. Casalnuovo, A. Altomare, G. Aldini, et al., Lipid peroxidation in atherosclerotic cardiovascular diseases, Antioxidants Redox Signal. 34 (2021) 49–98.
[7] M. Jaganjac, L. Milkovic, A. Gegotek, M. Cindric, K. Zarkovic, E. Skrzydlewska, et al., The relevance of pathophysiological alterations in redox signaling of 4-hydroxynonenal for pharmacological therapies of major stress-associated diseases, Free Radic. Biol. Med. 157 (2020) 128–153.
[8] Z. Qiang, H. Dong, Y. Xia, D. Chai, R. Hu, H. Jiang, Nrf2 and stat3 alleviates ferroptosis-mediated iir-ali by regulating slc7a11, Oxid. Med. Cell. Longev. 2020 (2020) 5146982.
[9] X. Jiang, B.R. Stockwell, M. Conrad, Ferroptosis: mechanisms, biology and role in disease, Nat. Rev. Mol. Cell Biol. 22 (2021) 266–282.
[10] S.J. Dixon, K.M. Lemberg, M.R. Lamprecht, R. Skouta, E.M. Zaitsev, C.E. Gleason, et al., Ferroptosis: an iron-dependent form of nonapoptotic cell death, Cell 149 (2012) 1060–1072.
[11] T. Bai, M. Li, Y. Liu, Z. Qiao, Z. Wang, Inhibition of ferroptosis alleviates atherosclerosis through attenuating lipid peroxidation and endothelial dysfunction in mouse aortic endothelial cell, Free Radic. Biol. Med. 160 (2020) 92–102.
[12] F. Vinchi, G. Porto, A. Simmelbauer, S. Altamura, S.T. Passos, M. Garbowski, et al., Atherosclerosis is aggravated by iron overload and ameliorated by dietary and pharmacological iron restriction, Eur. Heart J. 41 (2020) 2681–2695.
[13] A. Cuadrado, G. Manda, A. Hassan, M.J. Alcaraz, C. Barbas, A. Daiber, et al., Transcription factor nrf2 as a therapeutic target for chronic diseases: a systems medicine approach, Pharmacol. Rev. 70 (2018) 348–383.
[14] A.T. Dinkova-Kostova, R.V. Kostov, P. Canning, Keap1, the cysteine-based mammalian intracellular sensor for electrophiles and oxidants, Arch. Biochem. Biophys. 617 (2017) 84–93.
[15] A.T. Dinkova-Kostova, The role of sulfhydryl reactivity of small molecules for the activation of the keap1/nrf2 pathway and the heat shock response, Sci. Tech. Rep. 2012 (2012) 606104.
[16] J. Mimura, K. Itoh, Role of nrf2 in the pathogenesis of atherosclerosis, Free Radic. Biol. Med. 88 (2015) 221–232.
[17] E.H. Kobayashi, T. Suzuki, R. Funayama, T. Nagashima, M. Hayashi, H. Sekine, et al., Nrf2 suppresses macrophage inflammatory response by blocking proinflammatory cytokine transcription, Nat. Commun. 7 (2016) 11624.
[18] S.B. Wall, R. Li, B. Butler, A.R. Burg, H.M. Tse, J.L. Larson-Casey, et al., Auranofin-mediated nrf2 induction attenuates interleukin 1 beta expression in alveolar macrophages, Antioxidants 10 (2021).
[19] B. Chen, Y. Lu, Y. Chen, J. Cheng, The role of nrf2 in oxidative stress-induced endothelial injuries, J. Endocrinol. 225 (2015) R83–R99.
[20] H.P. Zhang, F.L. Zheng, J.H. Zhao, D.X. Guo, X.L. Chen, Genistein inhibits ox-ldl-induced vcam-1, icam-1 and mcp-1 expression of huvecs through heme oxygenase-1, Arch. Med. Res. 44 (2013) 13–20.
[21] A.L. Levonen, M. Inkala, T. Heikura, S. Jauhiainen, H.K. Jyrkkanen, E. Kansanen, et al., Nrf2 gene transfer induces antioxidant enzymes and suppresses smooth muscle cell growth in vitro and reduces oxidative stress in rabbit aorta in vivo, Arterioscler. Thromb. Vasc. Biol. 27 (2007) 741–747.
[22] B. Barajas, N. Che, F. Yin, A. Rowshanrad, L.D. Orozco, K.W. Gong, et al., Nf-e2-related factor 2 promotes atherosclerosis by effects on plasma lipoproteins and cholesterol transport that overshadow antioxidant protection, Arterioscler. Thromb. Vasc. Biol. 31 (2011) 58–66.
[23] N. Harada, K. Ito, T. Hosoya, J. Mimura, A. Maruyama, N. Noguchi, et al., Nrf2 in bone marrow-derived cells positively contributes to the advanced stage of atherosclerotic plaque formation, Free Radic. Biol. Med. 53 (2012) 2256–2262.
[24] A.K. Ruotsalainen, M. Inkala, M.E. Partanen, J.P. Lappalainen, E. Kansanen, P. I. Mäkinen, et al., The absence of macrophage nrf2 promotes early atherogenesis, Cardiovasc. Res. 98 (2013) 107–115.
[25] M. Stemmer, T. Thumberger, M. Del Sol Keyer, J. Wittbrodt, J.L. Mateo, Cctop: an intuitive, flexible and reliable crispr/cas9 target prediction tool, PLoS One 10 (2015) e0124633.
[26] K. Varadi, S. Michelfelder, T. Korff, M. Hecker, M. Trepel, H.A. Katus, et al., Novel random peptide libraries displayed on aav serotype 9 for selection of endothelial cell-directed gene transfer vectors, Gene Ther. 19 (2012) 800–809.
[27] L. Wang, J.Y. Luo, B. Li, X.Y. Tian, L.J. Chen, Y. Huang, et al., Integrin-yap/taz-jnk cascade mediates atheroprotective effect of unidirectional shear flow, Nature 540 (2016) 579–582.
[28] W. Song, C.L. Zhang, L. Gou, L. He, Y.Y. Gong, D. Qu, et al., Endothelial tfeb (transcription factor eb) restrains ikk (iκb kinase)-p65 pathway to attenuate vascular inflammation in diabetic db/db mice, Arterioscler. Thromb. Vasc. Biol. 39 (2019) 719–730.
[29] C.K. Cheng, X. Lin, Y. Pu, J.K.Y. Tse, Y. Wang, C.L. Zhang, et al., Sox4 is a novel phenotypic regulator of endothelial cells in atherosclerosis revealed by single-cell analysis, J. Adv. Res. 43 (2023) 187–203.
[30] P. Libby, Inflammation in atherosclerosis, Nature 420 (2002) 868–874.
[31] P. Libby, Inflammation in atherosclerosis, Arterioscler. Thromb. Vasc. Biol. 32 (2012) 2045–2051.
[32] Y. Baumer, S. McCurdy, T.M. Weatherby, N.N. Mehta, S. Halbherr, P. Halbherr, et al., Hyperlipidemia-induced cholesterol crystal production by endothelial cells promotes atherogenesis, Nat. Commun. 8 (2017) 1129.
[33] H. Feng, K. Schorpp, J. Jin, C.E. Yozwiak, B.G. Hoffstrom, A.M. Decker, et al., Transferrin receptor is a specific ferroptosis marker, Cell Rep. 30 (2020) 3411–3423.e3417.
[34] G. Miotto, M. Rossetto, M.L. Di Paolo, L. Orian, R. Venerando, A. Roveri, et al., Insight into the mechanism of ferroptosis inhibition by ferrostatin-1, Redox Biol. 28 (2020) 101328.
[35] H. Sawada, Y. Saito, N. Noguchi, Enhanced cd36 expression changes the role of nrf2 activation from anti-atherogenic to pro-atherogenic in apoe-deficient mice, Atherosclerosis 225 (2012) 83–90.
[36] E.L. Mills, D.G. Ryan, H.A. Prag, D. Dikovskaya, D. Menon, Z. Zaslona, et al., Itaconate is an anti-inflammatory metabolite that activates nrf2 via alkylation of keap1, Nature 556 (2018) 113–117.
[37] Z. Ungvari, S. Tarantini, A. Nyul-Toth, T. Kiss, A. Yabluchanskiy, T. Csipo, et al., Nrf2 dysfunction and impaired cellular resilience to oxidative stressors in the aged vasculature: from increased cellular senescence to the pathogenesis of age-related vascular diseases, Geroscience 41 (2019) 727–738.
[38] M.O. Grootaert, P.A. da Costa Martins, N. Bitsch, I. Pintelon, G.R. De Meyer, W. Martinet, et al., Defective autophagy in vascular smooth muscle cells accelerates senescence and promotes neointima formation and atherogenesis, Autophagy 11 (2015) 2014–2032.
[39] Z. Tan, H. Ren, Y. Liu, H. Yang, Q. Luo, X. Deng, Klf2 alleviates endothelial cell injury and inhibits the formation of thp-1 macrophage-derived foam cells by activating nrf2 and enhancing autophagy, Exp. Ther. Med. 24 (2022) 737.
[40] Y. Huang, W. Li, A.N. Kong, Anti-oxidative stress regulator nf-e2-related factor 2 mediates the adaptive induction of antioxidant and detoxifying enzymes by lipid peroxidation metabolite 4-hydroxynonenal, Cell Biosci. 2 (2012) 40.

[41] H.K. Jyrkkänen, E. Kansanen, M. Inkala, A.M. Kivelä, H. Hurttila, S.E. Heinonen, et al., Nrf2 regulates antioxidant gene expression evoked by oxidized phospholipids in endothelial cells and murine arteries in vivo, Circ. Res. 103 (2008) e1–e9.
[42] J. Jiang, Z.C. Mo, K. Yin, G.J. Zhao, Y.C. Lv, X.P. Ouyang, et al., Epigallocatechin-3-gallate prevents tnf-alpha-induced nf-kappab activation thereby upregulating abca1 via the nrf2/keap1 pathway in macrophage foam cells, Int. J. Mol. Med. 29 (2012) 946–956.
[43] B.K. Ooi, B.H. Goh, W.H. Yap, Oxidative stress in cardiovascular diseases: involvement of nrf2 antioxidant redox signaling in macrophage foam cells formation, Int. J. Mol. Sci. 18 (2017).
[44] A.D. Marais, Apolipoprotein e in lipoprotein metabolism, health and cardiovascular disease, Pathology 51 (2019) 165–176.
[45] G.S. Getz, C.A. Reardon, Do the apoe-/- and ldlr-/- mice yield the same insight on atherogenesis? Arterioscler. Thromb. Vasc. Biol. 36 (2016) 1734–1741.
[46] M. Bambouskova, L. Gorvel, V. Lampropoulou, A. Sergushichev, E. Loginicheva, K. Johnson, et al., Electrophilic properties of itaconate and derivatives regulate the iκbζ-atf3 inflammatory axis, Nature 556 (2018) 501–504.
[47] C.G. Peace, L.A. O'Neill, The role of itaconate in host defense and inflammation, J. Clin. Invest. (2022) 132.
[48] S. Nair, J.P. Huynh, V. Lampropoulou, E. Loginicheva, E. Esaulova, Irg1 expression in myeloid cells prevents immunopathology during m. Tuberculosis infection, J. Exp. Med. 215 (2018) 1035–1045.